



1 **First phytoplankton community assessment of the Kong**  
2 **Håkon VII Hav, Southern Ocean during austral autumn**

3

4 Hanna M. Kauko<sup>1</sup>, Philipp Assmy<sup>1</sup>, Ilka Peeken<sup>2</sup>, Magdalena Róžańska<sup>3</sup>, Józef M. Wiktor<sup>3</sup>,  
5 Gunnar Bratbak<sup>4</sup>, Asmita Singh<sup>5,6</sup>, Thomas J. Ryan-Keogh<sup>5</sup>, Sebastien Moreau<sup>1</sup>

6

7 <sup>1</sup> Norwegian Polar Institute, Fram Centre, Tromsø, Norway

8 <sup>2</sup> Alfred Wegener Institute Helmholtz Centre for Polar and Marine Research, Bremerhaven, Germany

9 <sup>3</sup> Institute of Oceanology, Polish Academy of Sciences, Sopot, Poland

10 <sup>4</sup> Department of Biological Sciences, University of Bergen, Bergen, Norway

11 <sup>5</sup> Southern Ocean Carbon and Climate Observatory (SOCCO), Council for Scientific and Industrial Research  
12 (CSIR), Cape Town, South Africa

13 <sup>6</sup> Department of Earth Sciences, Stellenbosch University, Stellenbosch, South Africa

14

15 Correspondence: Hanna M. Kauko, hanna.kauko@npolar.no; hanna.kauko@alumni.helsinki.fi

16

17 Key words: phytoplankton, chemotaxonomy, biodiversity, Weddell Gyre, carbon and silicon cycles

18

19 Key points:

- 20 1) A typical Southern Ocean open ocean phytoplankton community dominated by heavily silicified  
21 diatoms was observed in the Kong Håkon VII Hav in autumn 2019  
22 2) Blooms dominated by the diatom *Chaetoceros dichaeta* were observed in two of the sampling areas  
23 3) The other areas, mainly in a post-bloom phase, had high relative contribution from flagellates,  
24 predominantly from the Chl *c* -lineage

25



26 **Abstract**

27 We studied phyto- and protozooplankton community composition based on light microscopy, flow cytometry  
28 and photosynthetic pigment data in the Atlantic sector of the Southern Ocean during March 2019 (early austral  
29 autumn). Sampling was focused on the area east of the prime meridian in the Kong Håkon VII Hav, including  
30 Astrid Ridge, Maud Rise and a south-north transect at 6° E. Phytoplankton community composition throughout  
31 the studied area was characterized by oceanic diatoms typical of the iron-deplete High-Nutrient Low-  
32 Chlorophyll (HNLC) Southern Ocean. Topography and wind-driven iron supply likely sustained blooms  
33 dominated by the centric diatom *Chaetoceros dichaeta* at Maud Rise and at a station north of the 6° E transect.  
34 For the remainder of the 6° E transect diatom composition was similar to the previously mentioned bloom  
35 stations but flagellates dominated in abundance suggesting a post-bloom situation and likely top-down control by  
36 krill on the bloom-forming diatoms. Among flagellates, species with haptophyte-type pigments were the  
37 dominating group. At Astrid Ridge, overall abundances were lower and pennate were more numerous than  
38 centric diatoms, but the community composition was nevertheless typical for HNLC areas. The observations  
39 described here show that *C. dichaeta* can form blooms beyond the background biomass level and fuels both  
40 carbon export and upper trophic levels also within HNLC areas. This study is the first thorough assessment of  
41 phytoplankton communities in this region and can be compared to other seasons in future studies.

42 **1. Introduction**

43 Phytoplankton play an important role for marine food webs and biogeochemical cycles as primary producers and  
44 important mediators of the biological carbon pump. They are represented by a vast diversity of species that  
45 occupy various ecological niches and play different ecological and biogeochemical roles, with diatoms and  
46 haptophytes generally the main bloom-forming taxa at high latitudes (Arrigo et al., 1999; Assmy et al., 2013;  
47 Deppeler and Davidson, 2017; Tréguer et al., 2018). Hence, for a full characterization of an ecosystem and its  
48 biogeochemical function, it is important to investigate the phytoplankton species composition.

49 In the Southern Ocean, phytoplankton communities have been coarsely divided into two broad categories  
50 (Smetacek et al., 2004). Communities characteristic of iron-replete regions such as in coastal polynyas and near  
51 the Antarctic Peninsula and subantarctic islands (e.g. Blain et al., 2007; Pollard et al., 2009) are dominated by  
52 bloom forming species with a 'boom and bust' life cycle and high carbon export, and largely composed of  
53 weakly-silicified diatoms and *Phaeocystis antarctica*. The iron-limited High-Nutrient Low-Chlorophyll (HNLC)  
54 areas of the Antarctic Circumpolar Current (ACC) on the other hand are characterized by communities  
55 dominated by heavily silicified diatoms that largely drive the selective export of silicon (Assmy et al. 2013).  
56 Hence the impact on biogeochemical cycles differs dramatically depending on phytoplankton community  
57 composition. It however needs to be noted that within the diatom community representative of the iron-limited  
58 ACC certain species can support enhanced carbon export upon relief of iron limitation (Assmy et al., 2013;  
59 Smetacek et al., 2012). Outside of the bloom periods the community composition in areas such as the Weddell  
60 Gyre is typically characterized by smaller cells such as haptophyte flagellates (Vernet et al., 2019). The  
61 communities also have a varying role as prey and in the marine food webs: the large and heavily silicified  
62 bloom-forming species can be grazed by krill but are avoided by microzooplankton grazers, which can control  
63 the abundance of smaller prey (e.g. Irigoien et al., 2005; Löder et al., 2011; Smetacek et al., 2004).



64 This study was carried out as part of an ecosystem cruise in March 2019 to the Kong Håkon VII Hav, an area off  
65 Dronning Maud Land mainly east of the prime meridian that encompasses parts of the Eastern Weddell Gyre.  
66 The cruise observations and satellite chlorophyll *a* (Chl *a*) data have shown distinct phytoplankton phenologies  
67 in the region, such as between Astrid Ridge and Maud Rise (Kauko et al., 2021). Knowledge on the community  
68 composition complements our understanding of this regional variability. As Vernet et al. (2019) highlighted in  
69 their review about the Weddell Gyre, thorough characterizations of the phytoplankton community in this area are  
70 sparse, particularly in the area east of the prime meridian. This area is poorly studied, while spatial management  
71 processes require improved knowledge of the ecosystem. We used different methods, with each giving a  
72 complementary, though not complete picture of the phytoplankton community composition: light microscopy,  
73 flow cytometry and algal pigment analysis via High Performance Liquid Chromatography (HPLC) and the  
74 statistical method CHEMTAX (Mackey et al., 1996). The objectives of this study are to characterize the  
75 phytoplankton and other protists communities in Kong Håkon VII Hav in late summer – early autumn, delineate  
76 their spatial variability, and to discuss the environmental control of community composition.

## 77 2. Methods

### 78 2.1 Field sampling and laboratory analyses

79 The data for this study were collected during a research cruise with RV Kronprins Haakon to Kong Håkon VII  
80 Hav, in the Atlantic sector of Southern Ocean, from February to April 2019. Sampling stations were located at  
81 64.8 – 69.5° S and 2.3 – 13.5° E with Maud Rise, Astrid Ridge and a south-north transect at 6° E as the main  
82 focus areas (Fig. 1). In addition, two stations were sampled in between the areas: station 53 at 68.1° S, 6.0° E and  
83 station 54 at 68.5° S, 8.3° E. Station 53, though geographically close to the 6° E transect, showed much higher  
84 biomass and a distinct bloom event (Kauko et al., 2021; Moreau et al., in prep.) and was therefore considered  
85 separately.

86 Water samples were collected from multiple depths in the upper 100 m at a total of 37 stations (station numbers  
87 starting with 53) between 12 and 31 March in connection with CTD (conductivity-temperature-depth) casts with  
88 a 24-bottle or 12-bottle SBE 32 carousel water sampler.

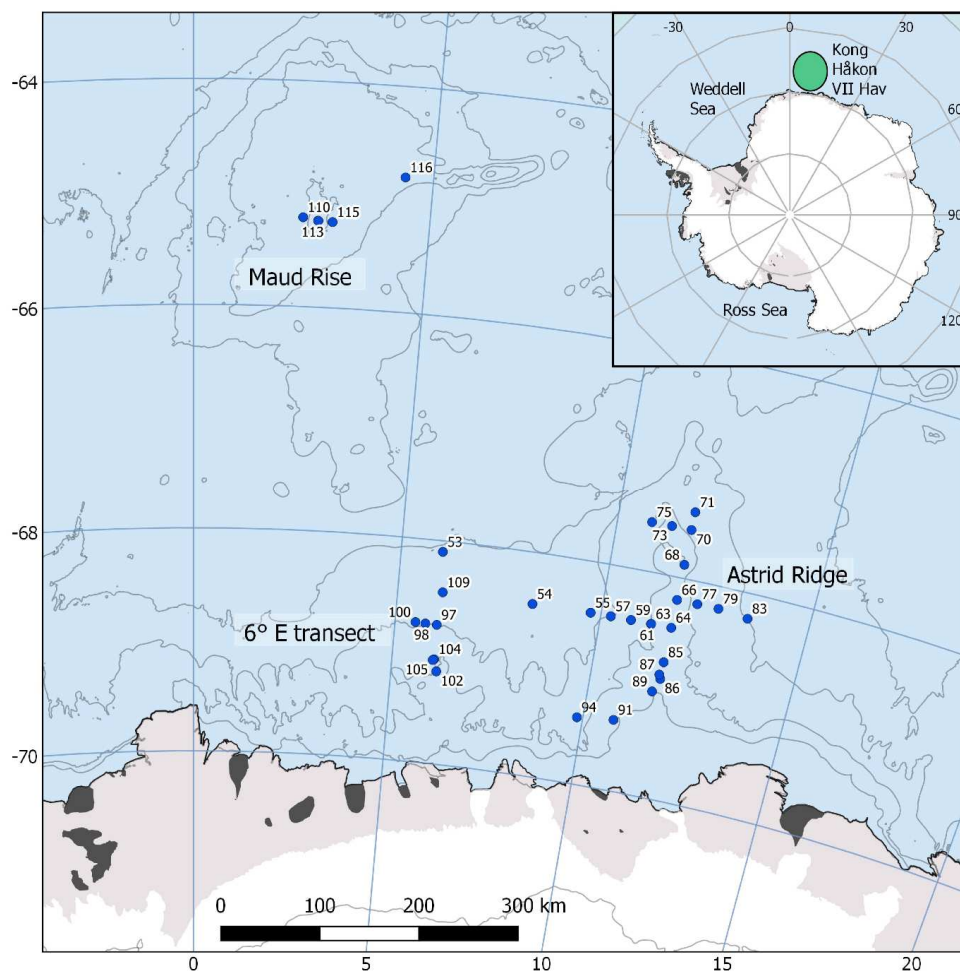
89 Samples for phytoplankton microscopy analyses (190 mL) were collected from 3 different depths (typically 10,  
90 25 or 40, and 75 m), filled into 200 mL brown glass bottles and fixed with glutaraldehyde and 20%  
91 hexamethylenetetramine-buffered formaldehyde at final concentrations of 0.1 and 1%, respectively, and  
92 thereafter stored cool and dark. For analysis, 10–50 mL subsample were settled in Utermöhl sedimentation  
93 chambers (HYDRO-BIOS®, Kiel, Germany) for 48 h and counted with a Nikon Ti-U inverted light microscope  
94 using the Utermöhl method (Edler and Elbrächter, 2010). Protists cells were counted in fields of view located  
95 along transects crossing the bottom of the chamber. In each sample, at least 50 cells of the dominant species  
96 were counted (error of ±28% according to Edler and Elbrächter, 2010).

97 Flow cytometry (FCM) samples (4.5 mL) for counting cells in small algal size classes (pico- and  
98 nanophytoplankton, 0.7 to 2 µm and 2 to 20 µm, respectively) were collected in cryovials from 5-6 different  
99 depths, fixed with glutaraldehyde (0.5% final concentration) and stored in -80° C until analyses at the University  
100 of Bergen. In the laboratory, samples were thawed, mixed gently, and analysed in an Attune™ NxT Acoustic



101 Focusing Cytometer (Invitrogen™, Thermo Fisher Scientific Inc. USA) equipped with a 50 mW 488 nm (blue)  
102 laser. Quantification and discrimination of the different phytoplankton size classes was done with the help of  
103 biparametric plots based on side scatter and red fluorescence.

104 Samples for algal pigment analysis (usually 1 L) were collected from 3 different depths (typically 10, 25 or 40,  
105 and 75 m), filtered on 0.7 µm GF/F filters (GE Healthcare, Little Chalfont, UK) with a gentle vacuum pressure  
106 (approximately -30 kPa), and immediately stored in the dark at -80° C. Pigments were measured and quantified  
107 with a Waters Alliance 2695 HPLC Separation Module connected to a Waters photodiode array detector (2,996).  
108 HPLC-grade solvents (Merck) and an Agilent Technologies Microsorb-MV3 C8 column (4.6 × 100 mm) was  
109 used for peak separation. The auto sampler module was kept at 4°C during the measurements. In total 100 µl  
110 sample were injected with an auto addition function of the system between sample and a 1 molar ammonium  
111 acetate solution in the ratio of 30:20:30:20. Peak identification and quantification was obtained with the  
112 EMPOWER software. More details about the solvents and gradient can be found in Tran et al. (2013). Overview  
113 of the taxonomical distribution of pigments is given in Jeffrey et al. (2011), Higgins et al. (2011) and the data  
114 sheets of Roy et al. (2011).



115

116 **Figure 1: Map of the study area. The CTD stations with water sampling are marked with blue circles. The sampling**  
117 **area is marked with a green ellipse in the insert. Map created with the help of Quantarctica (Norwegian Polar**  
118 **Institute, 2018).**

## 119 2.2 Statistical analyses

120 Similarity between the sampling areas in terms of the microscopy counts was evaluated with non-metric  
121 multidimensional scaling (NMDS) using the *isoMDS* function in the MASS package (Venables and Ripley,  
122 2002) and the R software (R Core Team, 2017). CTD samples down to 100 m depth with full taxonomical  
123 resolution were used for the analysis. Bray-Curtis dissimilarities (vegan package in R; Oksanen et al., 2017)  
124 were used for the scaling and abundances were square-root transformed prior to that to reduce the effect of high  
125 and uneven abundances. The dissimilarities between the groups were further tested statistically with the *anosim*  
126 function from the vegan package. Test result values (R values) close to 0, as opposed to 1, indicate random  
127 grouping. For the test considering differences between the sampling areas, the assumptions of heterogeneity and



128 similar sample size were not met, however, due to the lower range of dissimilarities occurring in the smaller-  
129 sized sample group Maud Rise (Fig. A1), the test tends to be overly conservative (Anderson and Walsh, 2013)  
130 and thus a significant result appears reliable.

131 Diversity in the phytoplankton community was investigated with the Shannon's diversity index ( $H'$ ; function  
132 *diversity* in the vegan package) and species richness (number of species, genera and size groups of unidentified  
133 taxa). Differences between the areas and sampling depths were tested with one-way Analysis of Variance  
134 (ANOVA; function *aov* in R). The assumptions of homoscedasticity were met in the models.

### 135 **2.3 CHEMTAX analysis**

136 Phytoplankton community composition was further investigated by applying a factor analysis program called  
137 CHEMTAX (Mackey et al., 1996), which allows to calculate the abundance of the various algal groups based on  
138 the measured marker pigments. As we had a large number of samples and no experimental or field information  
139 on local pigment ratios, the original approach (Mackey et al., 1996) was concluded to be more suitable than the  
140 Bayesian approach (Van den Meersche et al., 2008), according to Higgins et al. (2011). The software package  
141 CHEMTAX was obtained from Wright (2008).

142 The initial ratio matrix was based on literature. Pigment to Chl *a* ratios for prasinophytes, chlorophytes,  
143 cryptophytes, two pigment types of diatoms and peridinin-containing dinoflagellates were taken from the table in  
144 Wright et al. (2010), a study that was conducted close to our study area (between 30° to 80° E and south of 62°  
145 S), with the following modifications. Chl  $c_1$  was changed to Chl  $c_{1+2}$  (which is the resolution of our  
146 chromatographic results) with values taken from the CHEMTAX material (geometric means of reported ratios  
147 from the literature collected in Higgins et al., 2011). The values for 19'-butanoyloxyfucoxanthin (but-fuco),  
148 ratios for haptophytes pigment type 6 and for dinoflagellates pigment type 2 (microscopy revealed dominance of  
149 *Gymnodinium* spp.) were taken from Table 6.1 in Higgins et al. (2011). Zeaxanthin was observed in only one  
150 sample and was omitted from the analysis. Diadinoxanthin, diatoxanthin and  $\beta,\beta$ -carotene were excluded  
151 because they are not very group-specific. Neoxanthin, prasinoxanthin and violaxanthin were not observed in the  
152 samples and were removed from the ratio matrix.

153 Haptophytes belong to several (8) different pigment types (Zapata et al., 2004) and in addition change their  
154 marker pigment content according to environmental conditions such as iron availability (van Leeuwe and Stefels,  
155 1998; Wright et al., 2010). Therefore, all haptophyte pigment types were initially tested with CHEMTAX runs  
156 on all samples (20 randomized ratio matrices, using the pigment ratios from the CHEMTAX material mentioned  
157 above as initial ratios). The pigment type 8 is typical in the Southern Ocean including the species *P. antarctica*,  
158 whereas coccolithophores belong to pigment type 6. Out of the eight different pigment types tested, including  
159 pigment types 6, 7 or 8 resulted in the lowest root mean square errors (RMSE; below 0.2). Pigment type 7  
160 includes e.g. the genus *Chrysochromulina* which is not typical in the Southern Ocean. Including both haptophyte  
161 type 6 and 8 (in different ratio range categories according to the CHEMTAX instructions) also resulted in a low  
162 RMSE, and for the categories with high ratio range for haptophyte type 6 the error was lowest and similar to  
163 when including only haptophyte type 6 (<0.15). However, coccolithophores should not be abundant this far  
164 south (Balch et al., 2016; Saavedra-Pellitero et al., 2014; Trull et al., 2018) and were not observed in the  
165 microscopy samples. Other prymnesiophytes were not abundant either – only *P. antarctica* was observed in only



166 three CTD samples. This taxon has a characteristic appearance and, if present in large quantities, would likely  
167 have been identified, whereas the majority of flagellates in the microscopy samples were classified as  
168 unidentified flagellates in the 3 to 7  $\mu\text{m}$  size range. Therefore, to simplify the analysis (e.g. to avoid having too  
169 many algal groups compared to pigments, Mackey et al., 1996) and to account for the unidentified status of this  
170 group, we have included only one haptophyte group in the final runs with the best-performing i.e. type 6 pigment  
171 ratios and called this “Haptophytes-6-like”. Silicoflagellates and chrysophytes, that were observed at low  
172 abundances in microscopy samples (maximum abundances of 3900 and 18200 cells  $\text{L}^{-1}$ , respectively), will also  
173 be included in the haptophyte pigment group, as they contain similar pigments, e.g., Chl *c*, fucoxanthin and its  
174 derivatives (Jeffrey et al., 2011).

175 In the preliminary analysis, it was also tested to separate the samples into different clusters. With all samples  
176 combined, including only the surface samples down to 10 m, or successively adding depth ranges one at a time  
177 did not improve the result in terms of the RMSE, compared to including all depths. Separating Maud Rise from  
178 the rest reduced the error, when different area clusters were tested with all samples. Trials indicated that dividing  
179 the Maud Rise samples into depth clusters may bring further improvements but as the number of samples was  
180 relatively small (in total 12 CTD samples from Maud Rise) they were kept as one cluster. Astrid Ridge had a  
181 larger number of samples (55 in total) and was divided into two clusters (above and below including 40 m;  
182 average mixed layer depth (MLD) was 34 m, Kauko et al., 2021) and separated from the rest, which reduced the  
183 error. For the 6° E transect, separating the surface samples did not reduce the error.

184 In total there were 98 samples from the CTD casts. In the clusters Maud Rise, Astrid Ridge surface, Astrid Ridge  
185 deep and other stations (stations 53, 54 and 6° E transect) there were 12, 26, 29 and 31 samples, respectively.  
186 After the 60 first runs for each of the clusters (using 60 randomized pigment ratio matrices based on the initial  
187 ratio matrix), the average output ratio matrix of the 6 best runs was used as the initial ratio matrix for the next 60  
188 runs. The reported results are the averaged output from the six best runs of this second step.

### 189 3. Results

#### 190 3.1 Microscopy

191 The microscopy data are shown here as averages per sampling area and for the most important taxa separately,  
192 whereas others are summed together into higher-level categories such as “Pennate diatoms (other)”. All taxa are  
193 listed in Table B1 together with median abundances and occurrence in the different sampling areas, and variance  
194 in data used for the averages (i.e., data from all samples) is shown in Fig. A2 and A3.

195 Two of the sampling locations had an active diatom bloom, with average diatom abundances at station 53 and  
196 Maud Rise reaching  $5.2 \times 10^5$  and  $7.5 \times 10^5$  cells  $\text{L}^{-1}$ , respectively (Fig. 2a), and Chl *a* data showing the highest  
197 biomass in the area (Fig. 3; Kauko et al., 2021). Most of the sampling areas were dominated by diatoms in terms  
198 of average abundances, most notably for the area represented by station 53 and Maud Rise (74 and 89 %,   
199 respectively), whereas at station 54 or Astrid Ridge the dominance was less pronounced (62 and 56 %), and the  
200 area along the 6° E transect was slightly dominated by flagellates (45 % flagellates compared to 36 % diatoms).  
201 At Maud Rise flagellates and dinoflagellates occurred in similar abundances whereas in the other areas,  
202 flagellates were more abundant than dinoflagellates, most notably so along the 6° E transect. Ciliates and



203 cyanobacteria (unidentified filamentous blue-green algae cf. *Anabaena* sp., see photo in Fig. A4) were also  
204 observed at very low abundances, especially the latter mainly at Astrid Ridge and along the 6° E transect. FCM  
205 biplots (Fig. A5) using orange fluorescence indicated the presence of cyanobacteria in the corresponding  
206 samples, however abundances were low and the filamentous nature of the cyanobacteria complicates  
207 interpretations for this method.

208 The dominance patterns were similar when abundances were averaged per depth interval (Fig. A6), but at Astrid  
209 Ridge diatoms formed less than half of the community (about 30 %) below 45 m where dinoflagellates were  
210 slightly more prominent (32 to 37 %). In contrast, along the 6° E transect diatoms dominated at 75 m and formed  
211 about half of the community at 50 m. In terms of abundances, phytoplankton were concentrated in the upper 40  
212 m at station 53 and Astrid Ridge, whereas along the 6° E transect the generally low abundances were more  
213 evenly distributed with depth and at Maud Rise the bloom extended deeper with relatively high cell numbers ( $4$   
214  $\times 10^5$  cells  $L^{-1}$ ) until 75 m.

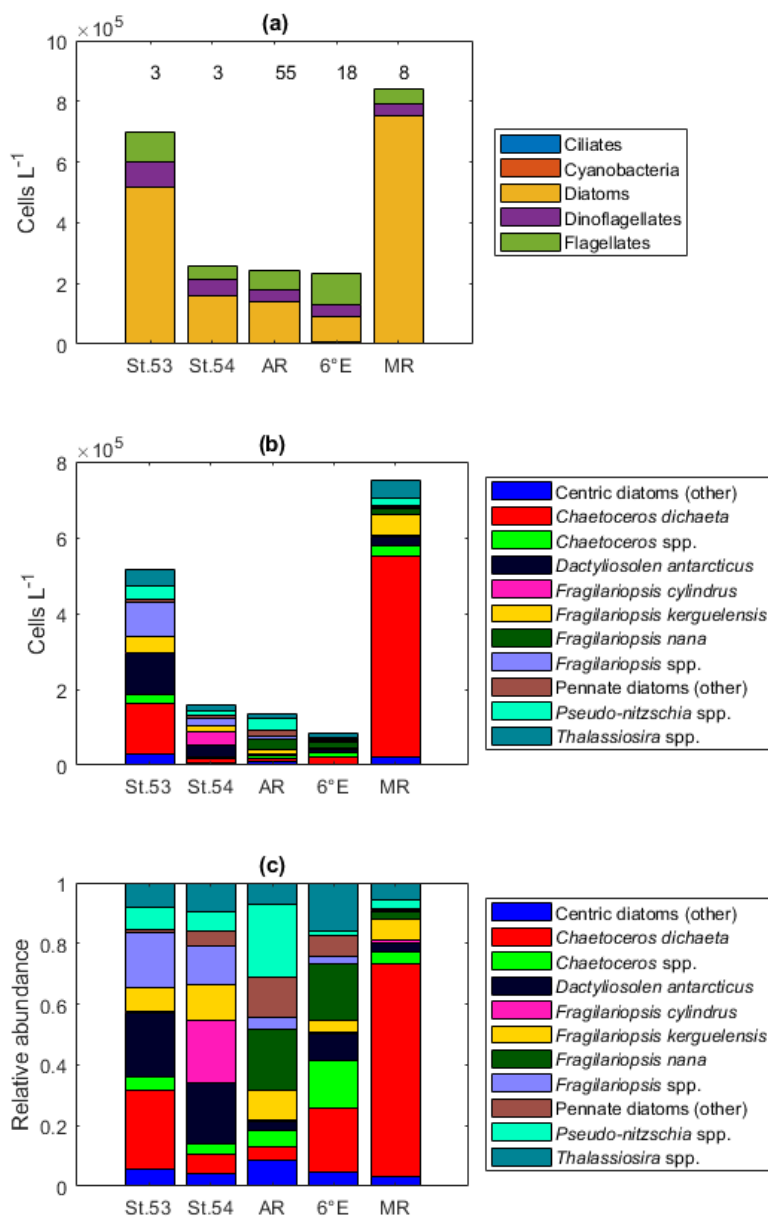
215 Among the diatoms, *Chaetoceros dichaeta* clearly dominated station 53 and Maud Rise communities down to 40  
216 and 50 m, respectively (Fig. 2b-c, 4 and A7). *Chaetoceros dichaeta* formed 59 % of the diatom community at 10  
217 m and 40 % at 40 m at station 53, i.e. it was the most abundant species at these depths. At Maud Rise, besides  
218 the surface samples, *C. dichaeta* dominated the diatom community at 100 m depth (at station 110; Fig. A8). This  
219 species was also an important component of the 6° E transect diatom community although at much lower  
220 abundances. In these other sampling areas not characterized by an active bloom (the 6° E transect, station 54 and  
221 Astrid Ridge), the abundances of various diatom species were more evenly distributed. Other important taxa  
222 were *Fragilariopsis* spp., *F. nana*, *F. kerguelensis*, *F. cylindrus*, *Dactyliosolen antarcticus*, *Chaetoceros* spp.  
223 and *Pseudo-nitzschia* spp. At Astrid Ridge and station 54, pennate diatoms (particularly *Fragilariopsis* spp. and  
224 *Pseudo-nitzschia* spp.) were more abundant than centric diatoms, with shares of 72 and 56 %, respectively. In  
225 other areas pennate diatoms contributed 14 to 34 %. Overall, there were 89 diatom taxa (at the genus or species  
226 level) identified during this research campaign.

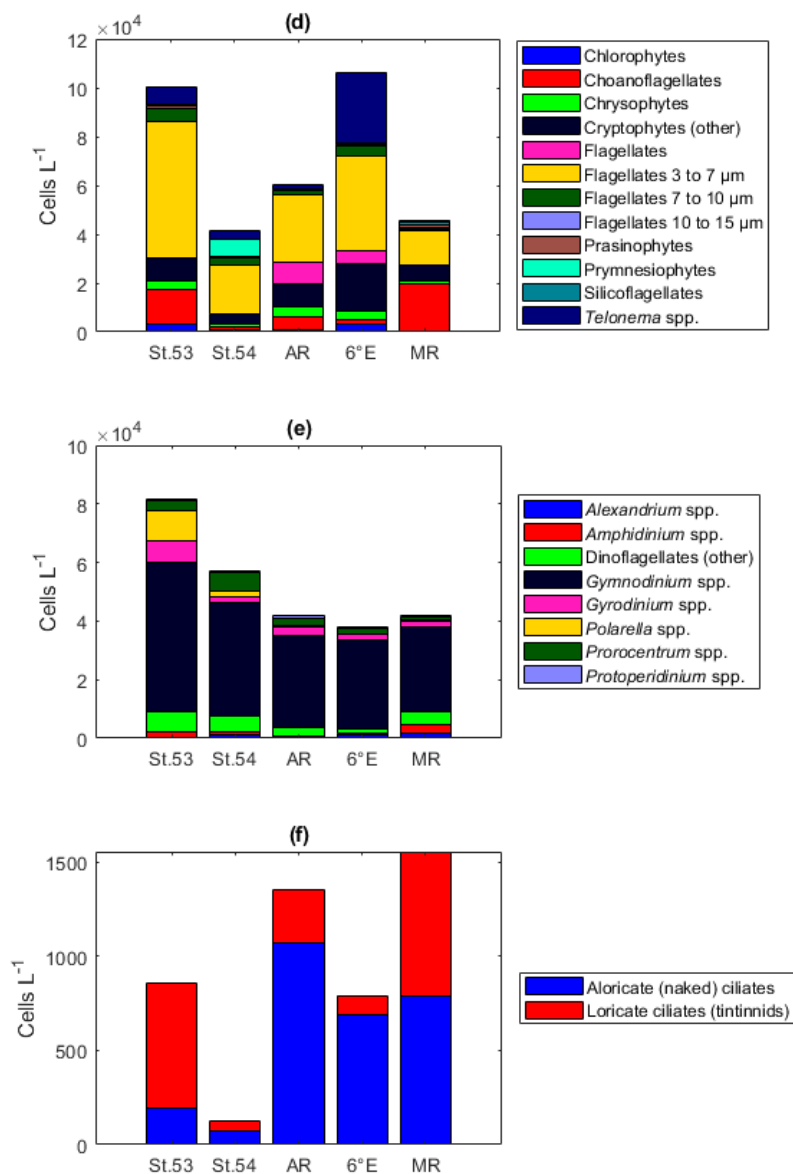
227 Maximum average abundances of flagellates were observed at station 53 and along the 6° E transect, with  $1.0 \times$   
228  $10^5$  and  $1.1 \times 10^5$  cells  $L^{-1}$ , respectively (Fig. 2d). Among the flagellates, a majority was categorized as  
229 unidentified flagellates in the size range 3 to 7  $\mu m$ . Cryptophytes and especially the genus *Telonema* were also a  
230 notable component of the flagellate community in many of the areas (in Fig. 2d cryptophytes and the genus  
231 *Telonema* are presented separately). Choanoflagellates (heterotrophic flagellates) were observed at relatively  
232 high numbers at station 53 and Maud Rise. *Phaeocystis antarctica* (the only prymnesiophyte species identified)  
233 was found at station 54 mainly at 40 m, but it was not an abundant species during the cruise, which was also  
234 confirmed by microscope analysis of live material from net samples taken from the upper 20 m at every CTD  
235 station during the cruise. Chlorophytes, chrysophytes, prasinophytes and silicoflagellates were also observed in  
236 minor numbers. The depth distribution of flagellates (figures not shown) was largely similar to the composition  
237 of the whole area averages, but choanoflagellates were most prominent at 25 m at Maud Rise.

238 Dinoflagellates belonged mainly to different, unidentified species of the genus *Gymnodinium* in all areas (Fig.  
239 2e) and at all depths (figures not shown). Additionally, the genera *Prorocentrum*, *Gyrodinium*, *Alexandrium*,  
240 *Amphidinium*, *Polarella* and *Protoperidinium* were also present. The maximum average dinoflagellates  
241 abundance was observed at station 53 ( $8.2 \times 10^4$  cells  $L^{-1}$ ).



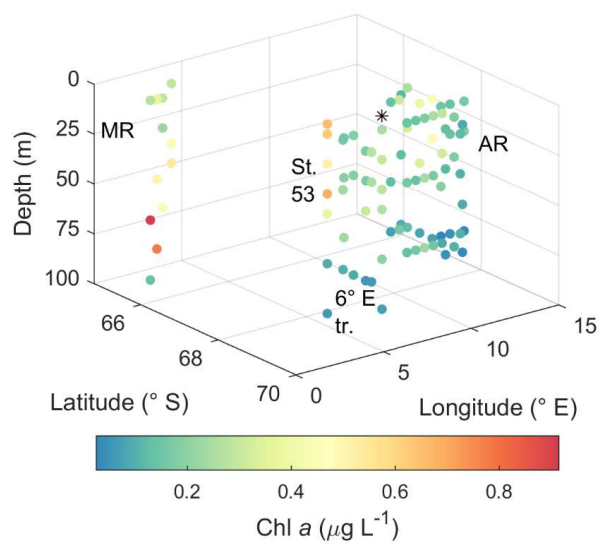
242 Ciliates were present in lower numbers (the maximum average abundance was 1500 cells L<sup>-1</sup> at Maud Rise; Fig.  
243 2f) but with several species (16 species or higher level taxa; Table B1). The most notable species were  
244 *Salpingella costata*, *Strombidium* spp., and *Lohmanniella oviformis*, as well as *Uronema marinum* at station 53  
245 and *Mesodinium rubrum* at station 54. At Astrid Ridge and along the 6° E transect, aloricate (naked) ciliates  
246 dominated in abundance (at station 54 the dominance was less pronounced), whereas at Maud Rise the  
247 abundances were even and at station 53 loricate ciliates (tintinnids) dominated (Fig. 2f). Ciliate abundances were  
248 lowest at station 54 (125 cells L<sup>-1</sup>).





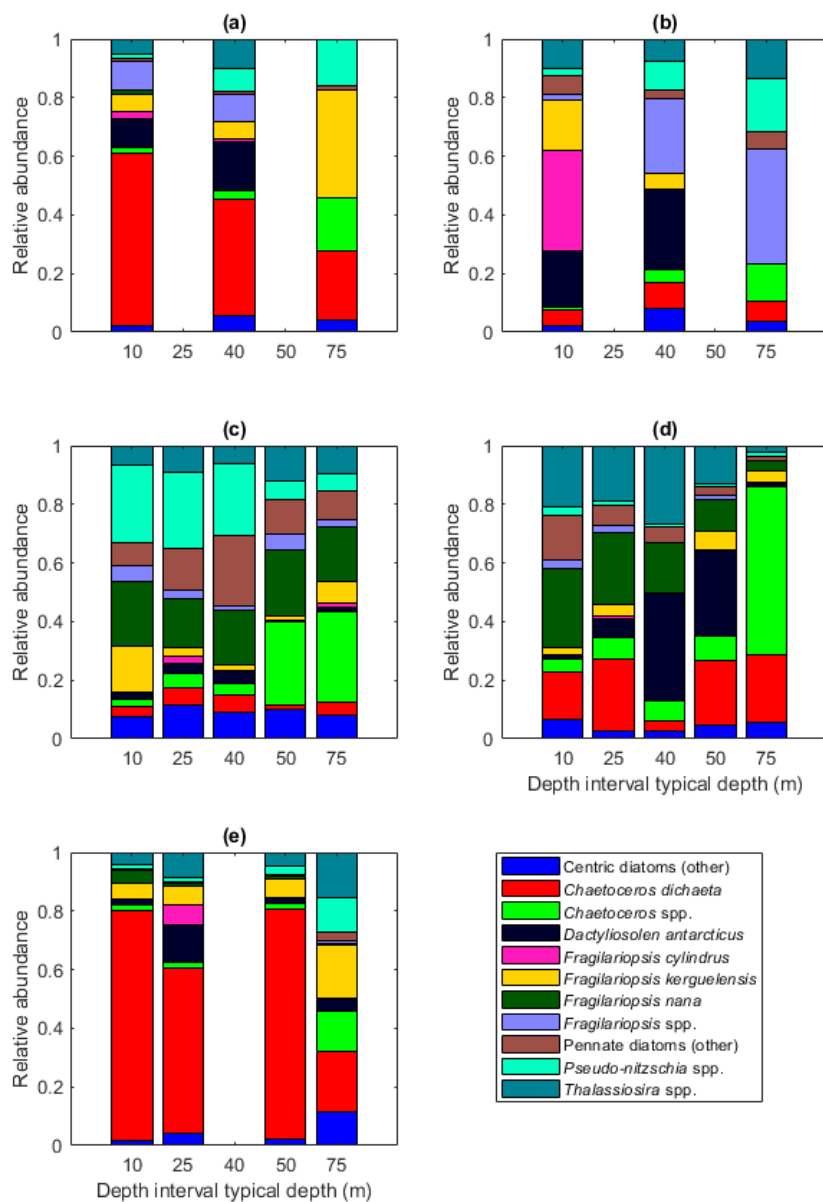
250

251 **Figure 2: Abundance of different protist groups and species for (a) main taxa, (b) diatoms, (c) relative abundance of**  
 252 **diatoms, (d) flagellates, (e) dinoflagellates and (f) ciliates. In (a), the number of samples used for the average**  
 253 **abundances is shown in the top of the figure (the numbers apply to all figures). In (c) and (d), the genera**  
 254 ***Fragilariopsis* and *Pseudo-nitzschia* belong to pennate diatoms, thus pennate diatoms are shown with colours**  
 255 **pink/yellow to cyan. St.53=station 53, St.54=station 54, AR=Astrid Ridge, 6E=6° E transect, MR=Maud Rise.**



256

257 **Figure 3: Horizontal and vertical distribution of phytoplankton biomass expressed as Chl *a* concentration. MR=Maud**  
258 **Rise, St. 53=station 53, AR=Astrid Ridge, 6° E tr.= 6° E transect. Station 54 is marked with a black asterisk.**



259

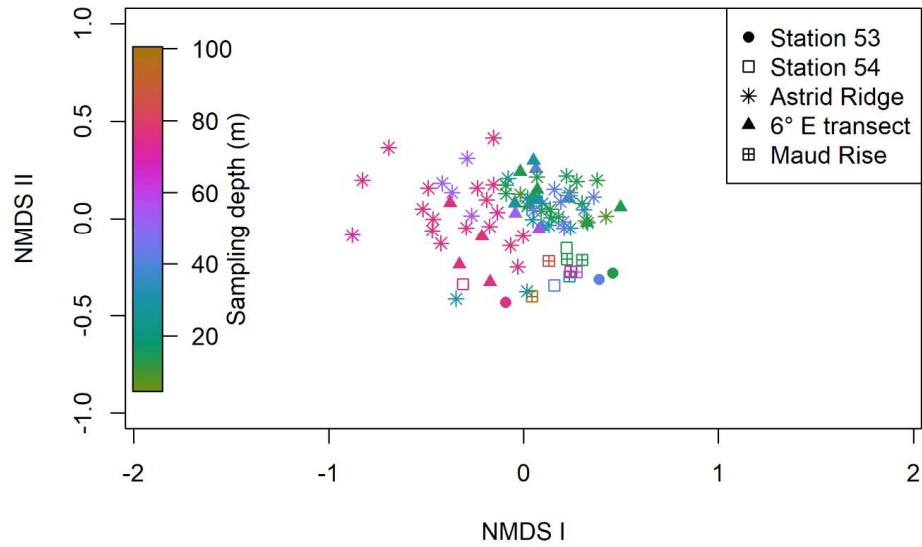
260 **Figure 4: Diatom relative abundance in the different sampling areas averaged per depth interval for (a) station 53, (b)**  
 261 **station 54, (c) Astrid Ridge, (d) 6° E transect and (e) Maud Rise. Depth intervals (with typical sampling depth in**  
 262 **brackets): 5-10 (10); 25-35 (25), 35-45 (40), 50-60, 65-85 (75) m.**



263 Clustering (NMDS) of the abundance results from the microscopy analysis showed that the communities in the  
264 different sampling areas (marked with different symbols in Fig. 5) did not separate into distinct clusters, but they  
265 appear located at different sides of the cluster, with station 53 and 54 and Maud Rise samples on one side and the  
266 Astrid Ridge and 6° E transect samples predominantly on the other side. In addition to the diatom blooms in the  
267 first two mentioned areas, this could also reflect a coastal to offshore pattern. However, the low R value of 0.15  
268 from the *anosim* test (significance 0.017) indicated overall a high similarity between the areas.

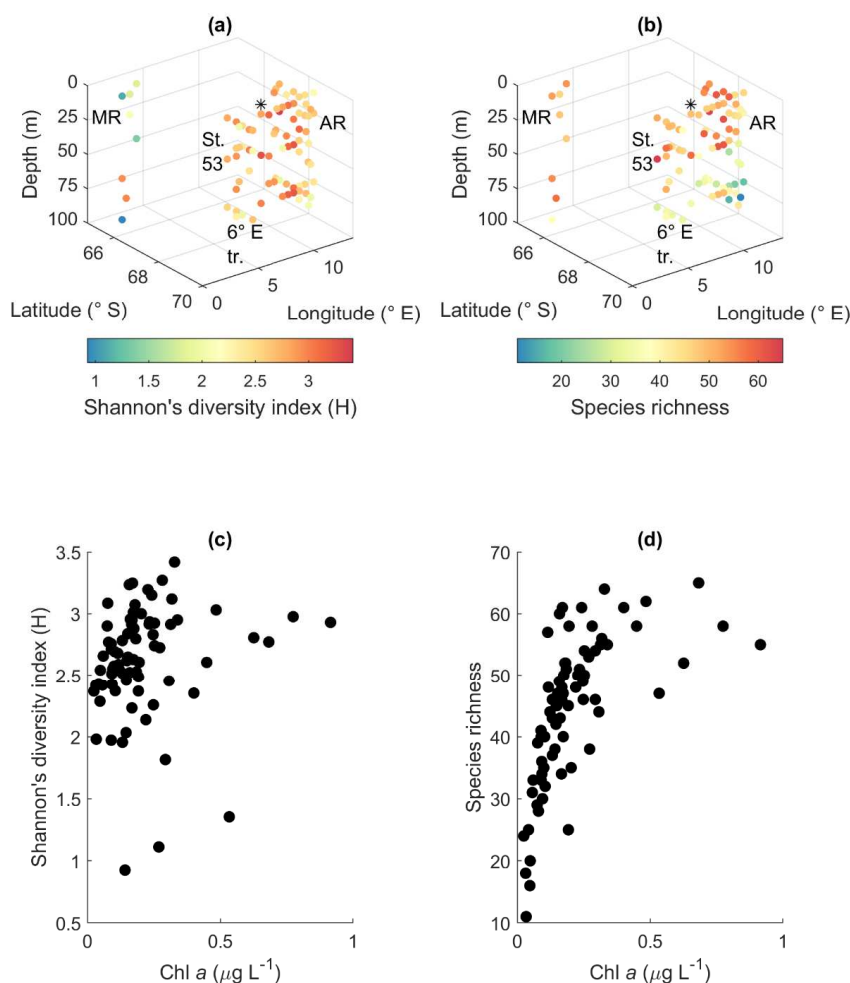
269 In addition, a separation along the sampling depth gradient (colour scale in Fig. 5) is clearly visible, with the  
270 surface samples (typically sampled at 25 m depth) and the deep samples (typically sampled at 75 m depth)  
271 located on different sides of the cluster. The *anosim* test indicated a somewhat higher degree of differentiation  
272 between the depth clusters (R value 0.27, significance 0.001) than between the sampling areas. In addition, when  
273 the NMDS analysis is performed on presence-absence data (Fig. A9), it is difficult to separate the areas, but the  
274 sampling depth pattern is still visible, though the samples are very condensed on the plot. Other categorizations  
275 included in the analysis, such as according to bottom depth, latitude or separation of Astrid Ridge into different  
276 areas (north, south, west and east parts of the Ridge), did not yield such clear patterns (figures not shown).

277 The Shannon's diversity index varied between 0.9 and 3.4, and the species richness between 11 and 65  
278 species/taxa. The biodiversity between the areas was relatively similar, but the most notable geographical  
279 patterns were that most depths at Maud Rise had a low diversity index, and that species richness in the other  
280 sampling areas was lower at depth than in the upper part of the water column (Fig. 6a and b). This was also  
281 visible in the statistical analysis of differences between groups: regarding the diversity index, the differences  
282 between areas were highly significant (p-value <0.001), but not between depth categories (p-value 0.32; the  
283 same depth categories were used as in the Fig. 4). A post-hoc Tukey test confirmed that Maud Rise differed from  
284 all other areas (p-value <0.02 for all comparisons). For species richness the inverse was found, differences  
285 between depth categories were significant (p-value <0.001) and not between the areas (0.69). A post-hoc Tukey  
286 test showed that the surface depth categories (10, 25 and 40 m) differed from the deeper categories (50 and 75 m;  
287 p-value for all comparisons <0.02, except for between 50 and 25 m where the p-value was 0.06), that is, species  
288 richness was significantly lower at depth (50 m and deeper). The means for the different areas were 2.7, 3.0, 2.7,  
289 2.6 and 1.9 for the diversity index and 49, 47, 44, 45 and 49 for species richness for station 53, station 54, Astrid  
290 Ridge, 6° E transect and Maud Rise, respectively. The mean diversity index was thus significantly lower at  
291 Maud Rise. The diversity index did not have a clear correlation with biomass, but species richness increased with  
292 increasing biomass up to maximum values of around 55–65 (Fig. 6c and d).



293

294 **Figure 5: Results of the NMDS clustering of the microscopy count samples. The colour shows the sampling depth and**  
295 **the different sampling areas are shown with different symbols, see legend. The stress value of the plot is 22 %.**



296

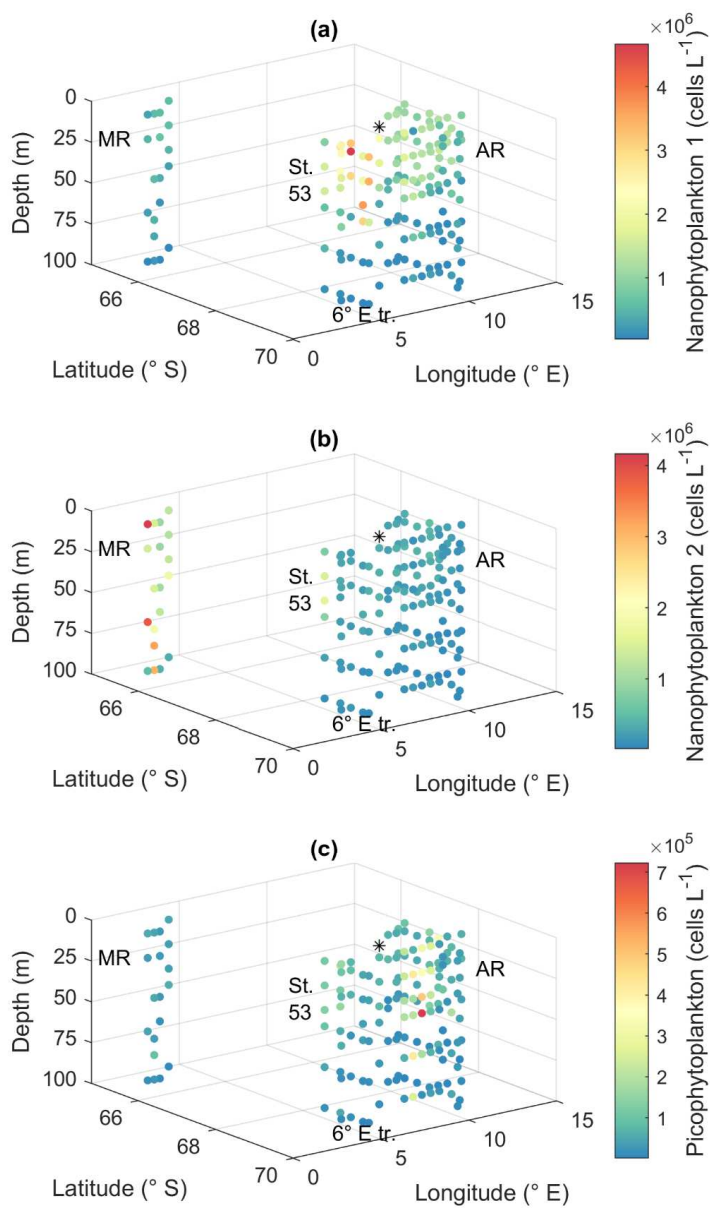
297 **Figure 6: Biodiversity according to the microscopy samples. (a) Shannon's diversity index, (b) species richness, (c)**  
298 **relationship between algal biomass (expressed in Chl a concentration) and Shannon's diversity index and (d) algal**  
299 **biomass and species richness. MR=Maud Rise, St. 53=station 53, AR=Astrid Ridge, 6° E tr.= 6° E transect. Station 54**  
300 **is marked with a black asterisk.**

### 301 3.2 Flow cytometry

302 Smaller nanophytoplankton (Nanophytoplankton 1; Fig. A5) showed the highest abundances along the 6° E  
303 transect, with abundances up to  $4.7 \times 10^6$  cells L<sup>-1</sup> (Fig. 7a), and lowest at Maud Rise. On the contrary, larger  
304 nanophytoplankton (Nanophytoplankton 2) were associated with Maud Rise and station 53 (up to  $4.2 \times 10^6$  cells



305 L<sup>-1</sup>; Fig. 7b). Maud Rise had high abundances also at depth, contrary to station 53. Some larger cells  
306 (Nanophytoplankton 2) were also observed on top of Astrid ridge (stations 66, 68 and 73), near the surface.  
307 Picophytoplankton abundance was lower than for nanophytoplankton (up to  $0.7 \times 10^6$  cells L<sup>-1</sup>; Fig. 7c), but a  
308 few stations on the west side of Astrid ridge (57, 59, 61) showed a distinct picophytoplankton population in the  
309 FCM biplots (Fig. A5).



310

311 **Figure 7: Flow cytometry results. Cell abundances of two groups of nanophytoplankton (a, b) and picophytoplankton**  
312 **(c). MR=Maud Rise, St. 53=station 53, AR=Astrid Ridge, 6° E tr.= 6° E transect. Station 54 is marked with a black**  
313 **asterisk.**



314 **3.3 Marker pigments**

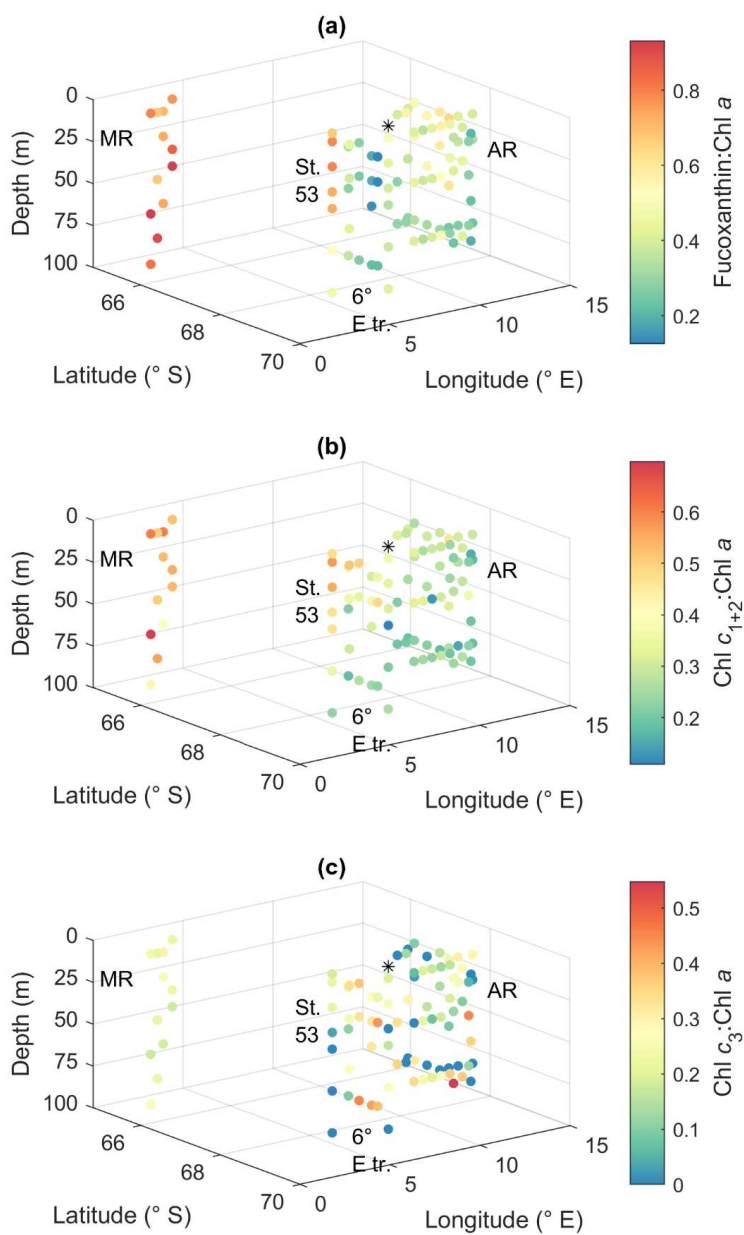
315 Pigment to Chl *a* ratios are presented in Fig. 8 and 9 and reported here, whereas the pigment concentrations are  
316 shown in Fig. A10 and A11. Chl *a* concentration ranged between 0.02 and 0.92  $\mu\text{g L}^{-1}$  (Fig. 3). The diatom  
317 blooms at Maud Rise and station 53, and the importance of flagellates at the 6° E transect were also visible in the  
318 pigment data.

319 Ratios of fucoxanthin, a typical pigment in diatoms, to Chl *a* were very high at Maud Rise and station 53, up to  
320 0.93 (Fig. 8a). The ratios were the lowest at the 6° E transect, with a minimum of 0.12. At Astrid Ridge the ratios  
321 were in between these values at around 0.5. The ratios of Chl  $c_{1+2}$  to Chl *a* were also the highest at Maud Rise  
322 and station 53, up to 0.70 and seemed thus to be primarily associated with fucoxanthin and diatoms (Fig. 8b).  
323 However, other Chl  $c_{1+2}$  containing groups were also likely present, as the ratios at the flagellate-dominated 6° E  
324 transect did not differ from the other areas as much as for fucoxanthin.

325 Chl  $c_3$  showed the highest pigment to Chl *a* ratio values at the 6° E transect and at depth at Astrid Ridge, up to  
326 0.55 (Fig. 8c). It was also found at Maud Rise at all depths, in the surface waters at station 53 and station 54, and  
327 at Astrid Ridge mainly in the middle of the ridge, from the surface to mid-depths. This pigment thus further  
328 indicates that flagellates were an important part of the 6° E transect community, as it is a major pigment e.g. in  
329 haptophytes. In addition, 19'-hexanoyloxyfucoxanthin (hex-fuco), another important pigment in haptophytes,  
330 showed clearly its highest pigment to Chl *a* ratio values at the 6° E transect, up to 1.01, and the lowest at Maud  
331 Rise (Fig. 8d). Another fucoxanthin derivative, but-fuco, that is mainly found in pelagophytes, silicoflagellates  
332 and some haptophytes, showed the highest pigment to Chl *a* ratio values at depth at the 6° E transect and Astrid  
333 Ridge, but values were low (Fig. 8e).

334 Diadinoxanthin, a carotenoid participating in the photoprotective xanthophyll cycle, occurred in the highest  
335 pigment to Chl *a* ratios close to the surface in all areas (up to 0.25), but at Maud Rise relatively high ratios were  
336 observed throughout the sampling depths (Fig. 8f). Diatoxanthin, its counterpart in the xanthophyll cycle, was  
337 observed in five samples at a much lower concentration (5–16 % of diadinoxanthin). It should be noted that  
338 although the samples were processed as quickly as possible, they were part of a larger sampling effort, and  
339 conversion from diatoxanthin to diadinoxanthin may have happened during the storage under dark conditions.

340 Peridinin (a major pigment in one of the dinoflagellate pigment classes), alloxanthin (a major pigment in  
341 cryptophytes), lutein (Chl *b*-lineage, e.g. chlorophytes and prasinophytes) and Chl *b* were observed in minor  
342 amounts in certain areas (Fig. 9): peridinin on the west side of Astrid Ridge (pigment to Chl *a* ratio up to 0.15),  
343 alloxanthin at the surface at a few stations of the 6° E transect and Astrid Ridge (up to 0.01), and lutein and Chl  
344 *b* at the 6° E transect (up to 0.04 and 0.06, respectively).  $\beta$ , $\beta$ -carotene is not very taxon-specific and did not show  
345 clear geographical patterns (pigment to Chl *a* ratio up to 0.05; Fig. A12). Zeaxanthin was only observed in one  
346 sample, in the surface (5 m) at station 70 at Astrid Ridge, in low concentration (ratio to Chl *a* was 0.02).

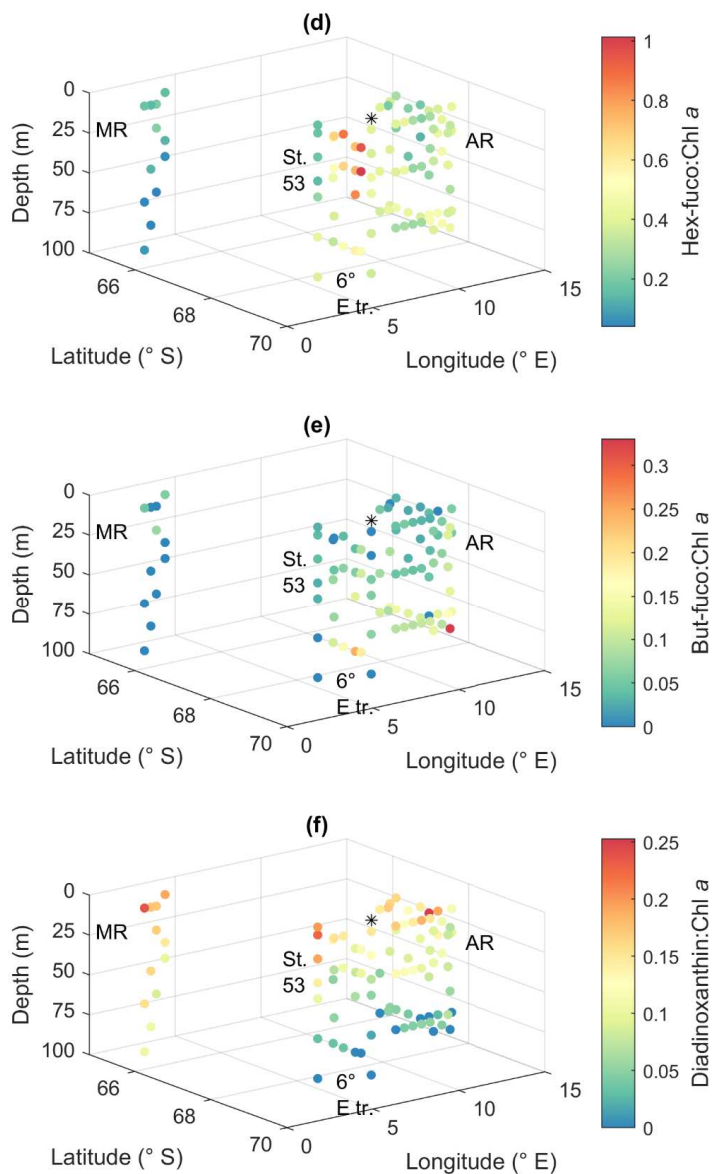


347

348

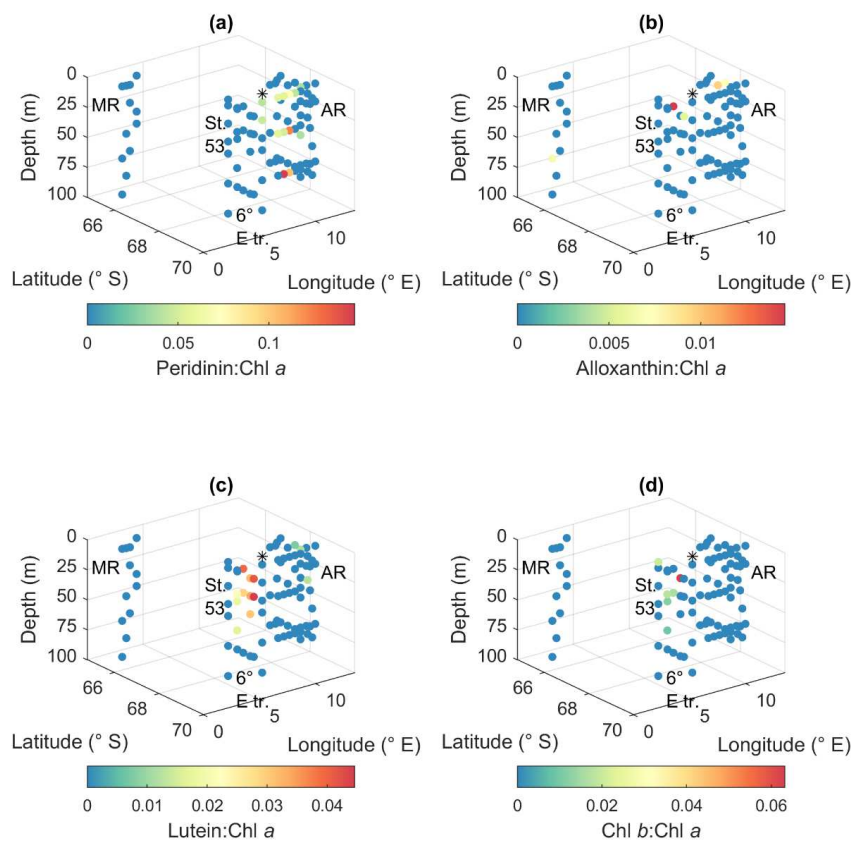


349



350

351 **Figure 8: Ratios of algal pigments to Chl a for (a) fucoxanthin, (b) Chl  $c_{1+2}$ , (c) Chl  $c_3$ , (d) hex-fuco, (e) but-fuco and (f)**  
352 **diadinoxanthin. MR=Maud Rise, St. 53=station 53, AR=Astrid Ridge, 6° E tr.= 6° E transect. Station 54 is marked**  
353 **with a black asterisk.**



354

355 **Figure 9: Ratios of algal pigments to Chl a for (a) peridinin, (b) alloxanthin, (c) lutein and (d) Chl b. MR=Maud Rise,**  
356 **St. 53=station 53, AR=Astrid Ridge, 6° E tr.= 6° E transect. Station 54 is marked with a black asterisk.**

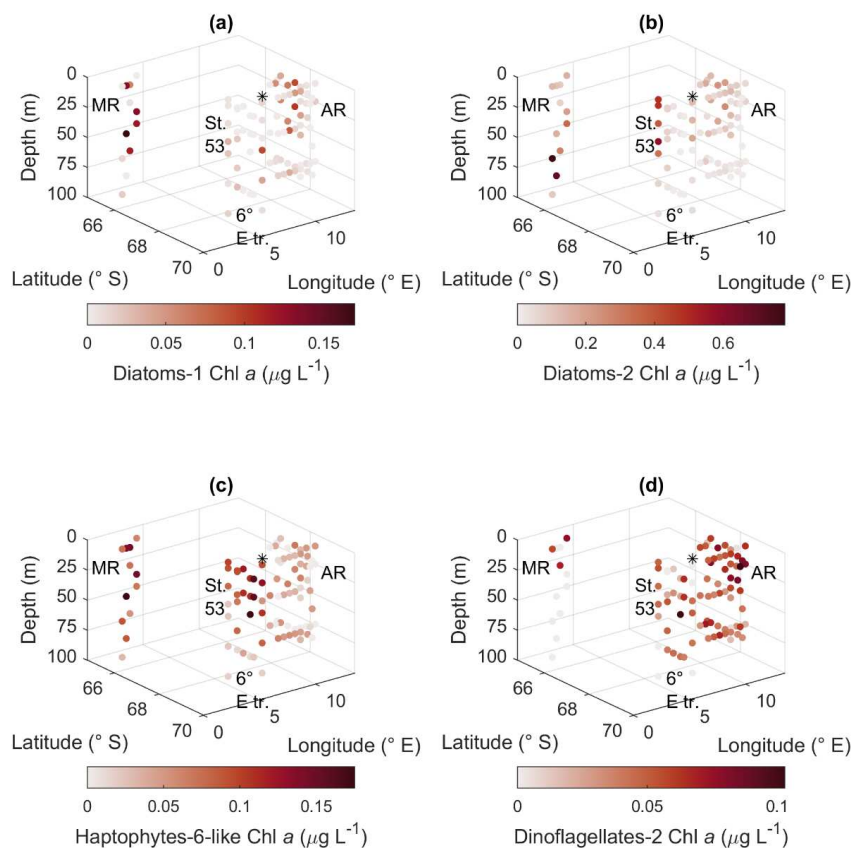
### 357 3.4 CHEMTAX analysis

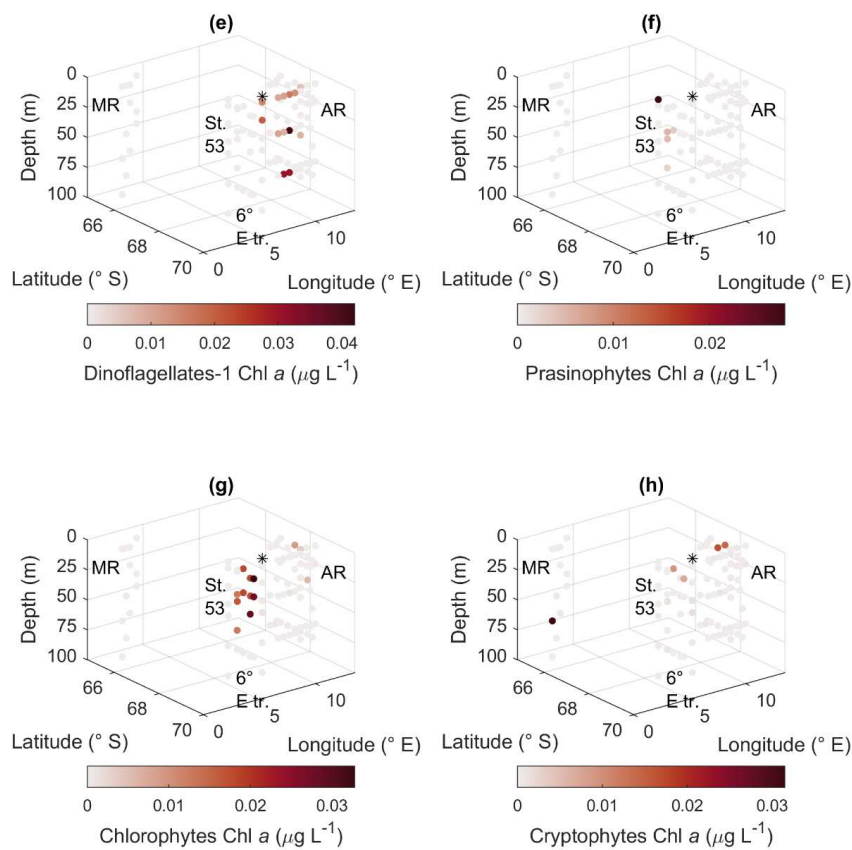
358 The CHEMTAX analysis is a way to distinguish and quantify the contribution of various phytoplankton groups  
359 based on the measured marker pigment concentrations. In total eight phytoplankton groups were included in the  
360 analysis based on prior knowledge from the microscopy results and the literature. Clear geographical patterns  
361 were observed in the distribution of the groups in line with the other phytoplankton data sources. Diatoms  
362 pigment type 2 (diatoms containing Chl  $c_3$ ) had the highest biomass, followed by diatoms type 1 and the  
363 haptophyte-like group (Fig. 10). Diatoms type 1 ranged up to  $0.17 \mu\text{g Chl } a \text{ L}^{-1}$  and had the highest values in the  
364 upper water column at Astrid Ridge and Maud Rise. Diatoms type 2 were most prominent at station 53 and at  
365 depth at Maud Rise with a maximum value of  $0.78 \mu\text{g Chl } a \text{ L}^{-1}$ . The haptophytes-6-like had the highest values  
366 at Maud Rise and the upper water column at the 6° E transect with a maximum value of  $0.18 \mu\text{g Chl } a \text{ L}^{-1}$ , but



367 clear presence also at Astrid Ridge. Of the dinoflagellate groups, type 2 had higher biomass and was present in  
368 all areas, though only at the surface at Maud Rise, with a maximum value of  $0.10 \mu\text{g Chl } a \text{ L}^{-1}$ . Occurrence of  
369 dinoflagellates type 1 (peridinin-containing dinoflagellates), prasinophytes, chlorophytes and cryptophytes in the  
370 CHEMTAX results (Fig. 10) followed closely the distribution of their respective marker pigments (Fig. 9) and  
371 was correspondingly scattered and scarce. A maximum value of  $0.04 \mu\text{g Chl } a \text{ L}^{-1}$  was found for dinoflagellates  
372 type 1 and  $0.03 \mu\text{g Chl } a \text{ L}^{-1}$  for the other three groups. From the Chl *b*-containing groups, chlorophytes were  
373 more abundant than prasinophytes with a clear presence along the  $6^\circ \text{ E}$  transect.

374 The final RMSE for the clusters Maud Rise, Astrid Ridge surface, Astrid Ridge deep and other stations (stations  
375 53, 54 and  $6^\circ$  transect) was 0.017, 0.064, 0.080 and 0.069, respectively (average RMSE of the best 6 runs). The  
376 final output ratio matrices for each of the clusters are presented in Table 1 for potential use as initial ratio  
377 matrices in future studies in the area. It is noteworthy that differentiating the data between the sampling areas,  
378 and in some cases along the depth gradient, improved the results.





380

381 **Figure 10: CHEMTAX results for the different algal groups. (a) Diatoms type 1, (b) diatoms type 2, (c) haptophytes**  
382 **type 6-like, (d) dinoflagellates type 1, (e) dinoflagellates type 2, (f) prasinophytes, (g) chlorophytes and (h)**  
383 **cryptophytes. MR=Maud Rise, St. 53=station 53, AR=Astrid Ridge, 6° E tr.= 6° E transect. Station 54 is marked with**  
384 **a black asterisk.**



385 **Table 1** Initial pigment to Chl a ratios used in the CHEMTAX analysis and the final ratio matrices for each cluster  
 386 (average of the 6 best performing runs of the second step; see Methods).

<b>Initial ratios</b>	Chl_c3	Chlc_1-2	Peri	But-fuco	Fuco	Hex-fuco	Allo	Lut	Chl_b	Chl_a
Prasinophytes	0	0	0	0	0	0	0	0.0066	0.55	1
Chlorophytes	0	0	0	0	0	0	0	0.23	0.15	1
Cryptophytes	0	0.17	0	0	0	0	0.21	0	0	1
Diatoms-1	0	0.09	0	0	1.04	0	0	0	0	1
Diatoms-2	0.016	0.22	0	0	0.83	0	0	0	0	1
Dinoflagellates-1	0	0.23	0.82	0	0	0	0	0	0	1
Dinoflagellates-2	0.04	0.12	0	0.06	0.19	0.18	0	0	0	1
Haptophytes-6-like	0.18	0.18	0	0.005	0.23	0.47	0	0	0	1

**Final ratios**

<b>Maud Rise</b>	Chl_c3	Chlc_1-2	Peri	But-fuco	Fuco	Hex-fuco	Allo	Lut	Chl_b	Chl_a
Prasinophytes	0	0	0	0	0	0	0	0.006	0.533	1
Chlorophytes	0	0	0	0	0	0	0	0.239	0.157	1
Cryptophytes	0	0.163	0	0	0	0	0.191	0	0	1
Diatoms-1	0	0.101	0	0	0.624	0	0	0	0	1
Diatoms-2	0.187	0.561	0	0	0.974	0	0	0	0	1
Dinoflagellates-1	0	0.221	0.714	0	0	0	0	0	0	1
Dinoflagellates-2	0.100	0.284	0	0.227	0.588	0.304	0	0	0	1
Haptophytes-6-like	0.495	0.809	0	0.003	0.557	0.404	0	0	0	1
<b>Astrid Ridge surface</b>	Chl_c3	Chlc_1-2	Peri	But-fuco	Fuco	Hex-fuco	Allo	Lut	Chl_b	Chl_a
Prasinophytes	0	0	0	0	0	0	0	0.006	0.507	1
Chlorophytes	0	0	0	0	0	0	0	0.260	0.153	1
Cryptophytes	0	0.179	0	0	0	0	0.211	0	0	1
Diatoms-1	0	0.112	0	0	1.232	0	0	0	0	1
Diatoms-2	0.015	0.324	0	0	0.429	0	0	0	0	1
Dinoflagellates-1	0	0.219	0.802	0	0	0	0	0	0	1
Dinoflagellates-2	0.031	0.209	0	0.142	0.256	0.576	0	0	0	1
Haptophytes-6-like	0.943	0.392	0	0.012	0.502	0.795	0	0	0	1
<b>Astrid Ridge deep</b>	Chl_c3	Chlc_1-2	Peri	But-fuco	Fuco	Hex-fuco	Allo	Lut	Chl_b	Chl_a
Prasinophytes	0	0	0	0	0	0	0	0.007	0.475	1
Chlorophytes	0	0	0	0	0	0	0	0.220	0.136	1
Cryptophytes	0	0.156	0	0	0	0	0.226	0	0	1
Diatoms-1	0	0.088	0	0	1.014	0	0	0	0	1
Diatoms-2	0.016	0.276	0	0	0.463	0	0	0	0	1
Dinoflagellates-1	0	0.233	0.765	0	0	0	0	0	0	1
Dinoflagellates-2	0.035	0.219	0	0.263	0.170	0.723	0	0	0	1
Haptophytes-6-like	0.728	0.240	0	0.007	0.379	0.336	0	0	0	1



Other stations	Chl_c3	Chlc_1-2	Peri	But-fuco	Fuco	Hex-fuco	Allo	Lut	Chl_b	Chl_a
Prasinophytes	0	0	0	0	0	0	0	0.007	0.400	1
Chlorophytes	0	0	0	0	0	0	0	0.306	0.096	1
Cryptophytes	0	0.190	0	0	0	0	0.236	0	0	1
Diatoms-1	0	0.088	0	0	1.030	0	0	0	0	1
Diatoms-2	0.017	0.378	0	0	0.608	0	0	0	0	1
Dinoflagellates-1	0	0.238	0.695	0	0	0	0	0	0	1
Dinoflagellates-2	0.301	0.414	0	0.358	0.403	0.573	0	0	0	1
Haptophytes-6-like	0.418	0.280	0	0.010	0.189	1.063	0	0	0	1

387

388 *Peri: peridinin; Fuco: fucoxanthin; Allo: alloxanthin; Lut: lutein.*

#### 389 4. Discussion

##### 390 4.1 Community patterns at the regional scale

391 The early autumn phyto- and protozooplankton community composition in Kong Håkon VII Hav was dominated  
 392 by diatoms and other algae from the Chl *c* -lineage, which is typical for the open Southern Ocean (e.g. Davidson  
 393 et al., 2010; Kang and Fryxell, 1993; van Leeuwe et al., 2015; Nöthig et al., 2009; Peeken, 1997; Smetacek et al.,  
 394 2004; Wright et al., 2010). Some differences in the relative abundance of the major taxa were observed between  
 395 the sampling areas, which will be discussed below. When it comes to biodiversity, phytoplankton species  
 396 richness was similar between the areas investigated. The Maud Rise bloom had lower diversity indices, which  
 397 can be attributed to the dominance of *C. dicheata* during the bloom (Vallina et al., 2014) and hence is likely not  
 398 reflecting persistent lower diversity at Maud Rise compared to the other areas – both species richness and  
 399 evenness in abundances between species are components of biodiversity. The diversity index and species  
 400 richness sampling area averages in our study were clearly higher than cluster averages in a community  
 401 composition study conducted at 30° – 80° E in austral summer (Davidson et al., 2010), and the diversity indices  
 402 were relatively high for the low biomass level compared to a global data compilation (Irigoiien et al., 2004).

403 Surprisingly, including the haptophytes pigment type 6 (“type species” coccolithophore *Gephyrocapsa huxleyi*,  
 404 formerly known as *Emiliana huxleyi*; Bendif et al., 2019) gave better results (lower error) in the preliminary  
 405 CHEMTAX analysis than including the pigment type 8 (e.g. *Phaeocystis*), and when including both pigment  
 406 types, type 6 was clearly more prominent. However, coccolithophores are not abundant this far south in the  
 407 Southern Ocean (Balch et al., 2016; Saavedra-Pellitero et al., 2014; Trull et al., 2018), which is confirmed in our  
 408 microscopy analysis. A few stations in the flow cytometry data may have had low abundances of  
 409 coccolithophores (not shown; based on high side-scattering and red fluorescence) but neither of these data  
 410 indicated a strong presence of this group throughout the study. Although blooms of *P. antarctica* are a prominent  
 411 feature in the marginal ice zones of the Ross Sea (Arrigo et al., 1999) and the Weddell Gyre (Vernet et al. 2019),  
 412 *P. antarctica* or other prymnesiophytes were not abundant in our microscopy samples. This is consistent with the  
 413 observation that blooms of *P. antarctica* are generally rare in the land-remote ACC (Smetacek et al. 2004) and  
 414 further supported by the low contribution of *P. antarctica* to bloom biomass in iron fertilization experiments



415 conducted in the iron-limited Southern Ocean (Boyd et al. 2008). Even the LOHAFEX iron fertilization  
416 experiment conducted in low silicate waters with a significant seed population of small initial *P. antarctica*  
417 colonies did not result in a bloom of this species, presumably because of strong top down control by copepod  
418 grazers (Schulz et al., 2018). Furthermore, blooms of *P. antarctica* seem to coincide with the sea ice retreat and  
419 ice edge (Davidson et al., 2010; Kang and Fryxell, 1993; Vernet et al., 2019). Our sampling effort was conducted  
420 later in the season (i.e., early autumn, at the onset of sea ice formation) and could therefore partly explain why  
421 the species was observed at low abundances. A subsequent cruise along the 6° E transect area earlier in the  
422 season (in December 2020–January 2021) observed higher abundances of *P. antarctica* (S. Moreau et al.,  
423 unpublished data).

424 Given the low contribution of both coccolithophores and *P. antarctica*, we have called the pigment group we  
425 included in the final CHEMTAX analysis as “Haptophytes-6-like” to acknowledge that the exact identity of this  
426 group is unclear and can contain other types of algae that have similar pigment ratios than the haptophyte 6  
427 group. The microscopy analysis indicated that the majority of the flagellates were different types of unidentified  
428 flagellates in the size group 3 to 7  $\mu\text{m}$  (note however that this group may and likely did also contain  
429 heterotrophic flagellates). It should also be noted that due to the similarity in pigments and pigment ratios, this  
430 pigment group will also contain silicoflagellates and chrysophytes. The former have a characteristic appearance  
431 and should have been reliably identified in the microscopy samples, thus their share in the pigment group should  
432 be correspondingly low as in the microscopy abundances. Unidentified chrysophytes on the contrary could have  
433 formed a considerable share of this pigment group. Chrysophytes were regularly observed in our microscopy  
434 samples, albeit not in high abundance. Unfortunately, pigment to Chl *a* ratio data are lacking for this group in the  
435 Southern Ocean. Cryptophytes, that were relatively abundant among flagellates in the microscopy samples, also  
436 contain similar pigments to haptophytes, but due to the low concentrations of their marker pigment alloxanthin  
437 they do not show up strongly in the CHEMTAX results. The discrepancies might be partly explained with the  
438 relatively small volume filtered (typically 1 L) for HPLC samples during this study, potentially leading to  
439 underestimation of pigments that are present in trace amounts. Thus, we recommend a higher filtration volume  
440 for further studies. All in all, our pigment composition was very similar (though with lower maximum  
441 concentrations) than in the study by Gibberd et al. (2013) that was conducted mainly at the prime meridian and  
442 the Weddell Sea in January – February one decade earlier.

443 Finally, picophytoplankton was not abundant in the area compared to nanophytoplankton – maximum  
444 picophytoplankton abundance was 15 % of maximum nanophytoplankton abundance, and only at certain  
445 stations, a distinct picophytoplankton occurrence was observed in the FCM biplots. The absence of coccoid  
446 cyanobacteria in the area contributes to low picophytoplankton abundance. Likewise, Rembauville et al. (2017)  
447 observed low picophytoplankton contribution (<20 % contribution to phytoplankton carbon) in the Indian sector  
448 in the Southern Ocean based on bio-optical observations from biogeochemical Argo floats, however the study  
449 area was further north than ours (around 50° S).

#### 450 **4.2 Vertical patterns**

451 Some of the data types and analyses indicated that the phytoplankton communities differed along the depth  
452 gradient, in addition to the spatial variability discussed in the next sections. Besides differences in biomass or



453 abundances (e.g., at Astrid Ridge the highest abundances were located in the upper 40 m), the species richness  
454 was significantly lower below 40 m. In the cluster analysis (Fig. 5), a separation along sampling depth gradient  
455 was visible in the figure (most notably separating the 25 m and 75 m depth categories), though further statistical  
456 tests didn't indicate large differences between communities at different depths. These patterns seem to suggest  
457 that the phytoplankton communities above and below the MLD (the average for all the stations was  $36 \pm 13$  m,  
458 Kauko et al., 2021) differed to some degree. As species richness correlated positively with biomass (Fig. 6d),  
459 which is a typical global pattern up to certain biomass level (Vallina et al., 2014), it is not surprising that species  
460 richness was lower at depth when surface biomass is typically higher. However, if other abundance patterns  
461 contributed to the depth separation was not easy to detect, as the species counts for the most abundant taxa in  
462 depth categories (Fig. A6 and A7) did not seem to differ to a great degree from the whole station or area  
463 averages (Fig. 2). A study from the Indian sector of the Southern Ocean concluded that phytoplankton  
464 communities at the deep Chl *a* maximum were not fundamentally different from surface mixed layer  
465 communities (Gomi et al., 2010), similarly to a study conducted between 30 and 80° E (Davidson et al., 2010).  
466 Moreover, the distinct sub-surface communities dominated by large diatoms found in the Southern Ocean are  
467 suggested to be linked to upstream surface blooms (Baldry et al., 2020).

468 At Maud Rise, vertical patterns were less clear as it seemed that the surface bloom was sinking based, e.g., on  
469 relatively high Chl *a* concentrations at depth and below the MLD (Kauko et al., 2021) and dampened  
470 diadinoxanthin vertical patterns compared to the other areas (Fig. 8f). This indicates that cells deeper in the water  
471 column had recently been exposed to upper water column light conditions. Furthermore, the diatom community  
472 at 100 m depth (at station 110) was dominated by *C. dicaeta*, whereas at 70 m at the same station the diatom  
473 community was more diverse (Fig. A8). There could be a somewhat separate community below the MLD (60 m  
474 at this station; Kauko et al., 2020), having access to more iron than the surface community and therefore thriving  
475 there (Baldry et al., 2020), which the sinking surface bloom could be "passing by" and then again dominating at  
476 100 m depth.

#### 477 **4.3 *Chaetoceros dicaeta* blooms associated with natural iron fertilization**

478 The different analyses – microscopic identification and pigments (especially fucoxanthin patterns and  
479 CHEMTAX results) – all show that a diatom bloom occurred at Maud Rise and station 53. The maximum  
480 diatom abundance was somewhat higher compared to a study in the north-western Weddell Sea in the same  
481 season (March):  $1.9 \times 10^6$  cells  $L^{-1}$  in our study compared to  $1.2 \times 10^6$  cells  $L^{-1}$  in Kang and Fryxell (1993). Both  
482 blooms observed in this study were dominated by *C. dicaeta*, which is an important and widespread species in  
483 the pelagic communities across the Southern Ocean (reviewed in Assmy et al., 2008). Maximum *C. dicaeta*  
484 abundance of  $1.6 \times 10^6$  cells  $L^{-1}$  was again higher than in the above mentioned study ( $0.4 \times 10^6$  cells  $L^{-1}$ ; Kang  
485 and Fryxell, 1993). This species seemed to belong to the diatoms pigment type 2, which was the most abundant  
486 of all groups and had maximum values at station 53 and Maud Rise. Likewise, in the study by Wright et al.  
487 (2010) east of our study area (30° – 80° E) the diatom type 2 was more widespread than the type 1 (though not  
488 linked to *C. dicaeta* dominance; Davidson et al., 2010), contrary to large parts of the prime meridian area and  
489 the Weddell Sea (Gibberd et al., 2013).



490 The observed bloom type belongs to the typical ecosystem of the open ocean iron-depleted areas of the Southern  
491 Ocean, where a few large, heavily silicified species are the main bloom-forming species (Lasbleiz et al., 2016;  
492 Smetacek et al., 2004). Grazing from copepods and protozoans exerts a strong selective pressure in these areas,  
493 and large diatom species with strong silicate armour and spines can more easily escape predation (Hansen et al.,  
494 1994; Irigoien et al., 2005; Löder et al., 2011; Pančić and Kiørboe, 2018; Smetacek et al., 2004). Indeed, small  
495 copepods (180–1000  $\mu\text{m}$ ) and protists were the main zooplankton groups in the area and more abundant at Maud  
496 Rise than in the other sampling areas (corresponding data for station 53 are lacking; Kauko et al., 2021).  
497 Furthermore, amongst the diatoms characteristic of the iron-limited ACC, *C. dictyota* seems to be quite  
498 responsive to elevated iron levels as it dominated blooms induced by iron fertilization experiments EIFEX and  
499 SOFEX south conducted in high silicate waters of the Southern Ocean during late austral summer (Assmy et al.,  
500 2013; Coale et al., 2004).

501 The observed phytoplankton community type is in contrast to iron-replete near-coastal areas where blooms are  
502 dominated by smaller and often spore-forming neritic diatoms e.g. from the genus *Thalassiosira* and the  
503 subgenus *Hyalochaete* within the genus *Chaetoceros* that can realize fast growth rates (Armand et al., 2008;  
504 Lasbleiz et al., 2016; Smetacek et al., 2004). Species belonging to these genera were observed in our samples,  
505 but only in low abundances. Although there are regional differences in bloom magnitude and, likely, iron input  
506 in our study area (Kauko et al., 2021; Moreau et al., in prep.), the iron input does not seem to be sufficient and  
507 persistent enough to sustain the coastal diatom communities characteristic of the iron-replete areas of the  
508 Southern Ocean. In this context also the inoculum is important, that is, coastal diatom species are likely to have  
509 low seeding abundance in oceanic waters at the start of the growth season, especially the spore forming taxa that  
510 tend to overwinter as resting spores on the seafloor. Indeed, the spore forming diatom *C. debilis* responded with  
511 exponential growth to iron fertilization in the EisenEx experiment in the polar frontal zone of the ACC but  
512 remained a minor component of the iron-induced diatom bloom because it started with a very low seed  
513 population (Assmy et al. 2007). Changes in the spatial extent of the iron-replete productive system and the iron-  
514 deplete HNLC system are reflected in diatom frustules preserved in Southern Ocean sediments covering the last  
515 glacial and interglacial time periods. During the more iron-rich glacial periods resting spores of the above  
516 mentioned *Chaetoceros* species dominated while the typical HNLC diatom *F. kerguelensis* dominated sediments  
517 representative of the interglacial period with less iron input to the Southern Ocean (Abelmann et al., 2006).

518 The blooms in our area were likely fuelled by upwelling-induced natural iron fertilization: at Maud Rise, the sea  
519 mount topography is suggested to lead to upwelling of nutrients (von Berg et al., 2020; Jena and Pillai, 2020;  
520 Kauko et al., 2021; de Steur et al., 2007), whereas in the area represented by station 53 wind patterns create  
521 suitable upwelling conditions and supply the area with additional, deep iron (Moreau et al., in prep.). Carbon  
522 export to the deep sea is typically low in the HNLC areas of the Southern Ocean while silica export is high due  
523 to the heavily silicified frustules of the dominant HNLC diatom taxa (Assmy et al., 2013; Smetacek et al., 2004).  
524 On the other hand, significant carbon export from open-ocean fertilized blooms has been observed (Smetacek et  
525 al., 2012) and attributed to mass mortality and aggregation of chain-forming oceanic *Chaetoceros* species,  
526 particularly *C. dictyota* (Assmy et al., 2013). In our study, the vertical Chl *a* profiles show that at Maud Rise the  
527 biomass, as Chl *a* concentration above 0.01  $\text{mg m}^{-3}$ , seemed to be sinking to approximately 300 m depth at the  
528 time of sampling (Kauko et al., 2021). Krill (which would be an important grazer of these large and spiny



529 colonies; Smetacek et al., 2004) was not observed in notable abundances at Maud Rise during the cruise (Kauko  
530 et al., 2021), which may indicate lower grazing pressure on the bloom and support vertical export as the main  
531 loss term. Indeed, fluxes of labile organic matter to the seafloor are elevated at Maud Rise compared to the  
532 surrounding waters (Sachs et al., 2009). On the contrary, at station 53 grazing presumably by krill played an  
533 important role for the bloom fate (Moreau et al., in prep.).

534 In addition to the diatom dominance, larger nanophytoplankton (Nanophytoplankton 2 in the FCM results) were  
535 a notable component of the community at Maud Rise and station 53 (unlike in the other sampling areas). None of  
536 the flagellate groups identified with microscopy correlated well with these results so the identity is unknown.  
537 Lastly, ciliates also showed patterns that were seemingly connected to the blooms and/or the nanophytoplankton  
538 patterns, namely the larger share of tintinnid ciliates at Maud Rise and station 53.

#### 539 **4.4 Dominance of pennate diatoms at Astrid Ridge**

540 Astrid Ridge and station 54 differed from the other sampling areas most notably by the more prominent role of  
541 pennate diatoms (56 to 72 % of total diatom abundance). Phytoplankton abundance was in general much lower at  
542 Astrid Ridge and station 54 than at Maud Rise, but diatoms were still more abundant than flagellates. The  
543 phytoplankton community at Astrid Ridge was likely in a post bloom situation (Kauko et al., 2021). Also in this  
544 area many of the dominant species fit into the concept of large, heavily silicified diatoms of the iron-deplete  
545 areas (see discussion in the previous section; Smetacek et al., 2004), and *C. dicaeta* was also an important  
546 species here. In terms of average abundance in all Astrid Ridge samples, the six most abundant taxa were the  
547 pennate diatoms *Pseudo-nitzschia* spp., *Fragilariopsis nana*, *F. kerguelensis* and *Thalassiothrix antarctica* and  
548 the centric diatoms *Thalassiosira* spp. and *C. dicaeta*.

549 Pennate diatoms are typically dominant in sea ice (Hop et al., 2020; van Leeuwe et al., 2018; Leu et al., 2015;  
550 Poulin et al., 2011). This was also true for our study, where two ice cores sampled along the 6° E transect  
551 showed strong dominance of pennate diatoms ( $\leq 95$  % of diatom abundance; Fig. A13). Furthermore, out of the  
552 20 dominant diatom species or genera in the ice cores and at Astrid Ridge (average of the samples down to 100  
553 m), 12 were shared between these two habitats (Table B2; see the table also for ice core method descriptions). It  
554 is however difficult to say whether the sea ice communities influenced the phytoplankton community  
555 composition, as observed in spring e.g. at the West Antarctic Peninsula (van Leeuwe et al., 2020), or if the sea  
556 ice reflected the water column community, but with some species succession towards ice specialists (Kauko et  
557 al., 2018), as species exchange between the habitats occurs both during sea ice melt and sea ice formation  
558 (Hardge et al., 2017). If the former was the case here, the later sea ice retreat at Astrid Ridge compared to many  
559 of the other sampling areas (Kauko et al., 2021) could introduce algae from the sea ice at a later stage in the  
560 growing season and possibly partly explain the dominance of pennate diatoms in this area. Due to the long sea  
561 ice period, sea ice algae could also have a prominent sediment seed bank in the area, which could introduce cells  
562 higher up in the water column through local current processes such as the strong tidal currents in this area  
563 (Kauko et al., 2021). This topic thus requires further study and is interesting also in the light of any possible  
564 costal to offshore gradients.

565 Astrid Ridge was most thoroughly sampled from all the sampling areas with a large number of CTD stations and  
566 samples, with some variation seen within this area. In particular a few stations on the western part of Astrid



567 Ridge showed distinct features, including the highest picophytoplankton abundances and peridinin  
568 concentrations of the entire sampling area. Future studies concentrating on the detailed current or food web  
569 patterns in this area could indicate which processes contributed to these observations. However, when the  
570 different parts of Astrid Ridge (southern, northern, western and eastern parts of the cross transect) were marked  
571 in the cluster analysis using microscopy counts (figures not shown), no clear patterns emerged, and the areas  
572 were mixed.

#### 573 **4.5 A flagellate-dominated post-bloom community**

574 Both FCM, pigment and microscopy data indicated that flagellates and the smaller nanophytoplankton were an  
575 important component of the phytoplankton community at the 6° E transect. According to the microscopy data,  
576 flagellates numerically dominated over diatoms, and the observed marker pigments pointed towards a diverse  
577 flagellate community. Except cryptophytes, flagellates remained to a large degree unidentified in the microscopy  
578 samples, but pigment data showed that algae from the Chl *c*- lineage were most abundant. These could have been  
579 haptophytes and possibly in addition chrysophytes (see Discussion section 4.1). Chl *b* containing algae were  
580 present in low concentrations.

581 The 6° E transect area, similarly to Astrid Ridge, typically experiences summer blooms, and the low biomass and  
582 abundances during this cruise likely point to a post-bloom situation (Kauko et al., 2021). Indeed, the importance  
583 of flagellates and pico- and nanophytoplankton is thought to be the typical situation e.g. in the Weddell Gyre  
584 (Vernet et al., 2019) or in the Southern Ocean in general (Buma et al., 1990; Detmer and Bathmann, 1997;  
585 Smetacek et al., 2004) outside the bloom periods, during which larger cells, mainly diatoms, dominate. The  
586 abundance of nanophytoplankton in our FCM samples was very similar to the suggested “background  
587 concentration” of  $2\text{--}4 \times 10^6$  cells L<sup>-1</sup> for the Southern Ocean (Detmer and Bathmann, 1997). Previous studies  
588 from Wright et al. (2010) and Davidson et al. (2010) observed somewhat further east of our study area (30° – 80°  
589 E) that the northern areas with most advanced blooms and likely depleted iron concentrations were dominated by  
590 nanoflagellates, and suggested that krill grazing contributed to the community composition as they are  
591 ineffective in feeding on the smaller organisms, as also pointed out by other studies (Granéli et al., 1993;  
592 Kopczynska, 1992). Kauko et al. (2021) hypothesized that blooms in our study area were at least partly  
593 terminated by krill grazing, as macronutrient concentrations in the upper water column were still sufficient to  
594 support phytoplankton production during the cruise (i.e. after the peak bloom), and short-term incubations  
595 indicated minimal iron limitation in the southern cruise area (Singh et al., in prep.).

596 Although station 53 was close to the 6° E transect, it showed a different relative community composition, which  
597 could be a result of the different bloom phase. The station 53 area typically has a late bloom according to a  
598 phenology analysis using satellite Chl *a* remote sensing data (Kauko et al., 2021) and was also during the cruise  
599 in an earlier bloom phase than the surrounding areas. These two areas were also separated by an oceanographic  
600 front (Moreau et al., in prep.). It can be speculated that the 6° E transect area had earlier experienced a *C.*  
601 *dichaeta* dominated bloom similar to Maud Rise and station 53 just north of this transect, as *C. dichaeta* had  
602 fairly high relative abundance (21 %) among diatoms along the 6° E transect.

603 There was possibly a south to north gradient visible in the diatom community along the 6° E transect (Fig. A14).  
604 The relative abundance of *C. dichaeta* increased at the northernmost station, i.e., towards station 53, whereas the



605 relative abundance of e.g. *F. nana* decreased. Additionally, lutein and hex-fuco showed higher pigment to Chl *a*  
606 ratios in the southern part of the transect. At the coast, several oceanographic features and processes can affect  
607 iron sources and the phytoplankton growth environment: the Antarctic Slope Current, glacial melt-related  
608 processes, shallower bottom topography and the occurrence of latent heat polynyas (e.g. Arrigo and van Dijken,  
609 2003; Dinniman et al., 2020; Dong et al., 2016). Differences between onshore and offshore communities have  
610 been observed east of the study area (between 30 and 80° E; Davidson et al., 2010). Future studies where  
611 sampling very close to the coast is possible will give further insights into the community composition in these  
612 areas. Due to heavy sea ice conditions, it was not possible to reach the coast during this cruise.

## 613 5. Conclusions

614 In this study, we have explored the phytoplankton community composition in a poorly studied area east of the  
615 prime meridian in the Southern Ocean, in the Kong Håkon VII Hav. The results indicate that the area has a  
616 typical open-ocean community composition with large, heavily silicified diatoms forming the blooms. These  
617 species traits are according to the literature a long-term evolutionary response to the heavy grazing pressure  
618 exerted by the micro- and mesozooplankton in the Southern Ocean. Furthermore, seasonal succession and bloom  
619 phase differences likely contributed to differences between the sampling areas, with post-bloom areas having a  
620 higher relative contribution by flagellates. Grazing (especially by krill) on bloom-forming species had likely  
621 shaped the community composition. The transient diatom blooms overlay a more stable flagellate-dominated  
622 background community.

623 The blooms described here were likely fuelled by natural iron fertilization driven by topography and wind-driven  
624 upwelling. Open ocean blooms triggered by local iron input cannot rival the more productive coastal systems of  
625 the Southern Ocean but enhance carbon export and feed a significant krill subpopulation. These results thus  
626 indicate that there exists a “middle ground” between the iron-replete coastal blooms and the iron-deplete status  
627 of the HNLC areas: oceanic blooms that are formed by some of the HNLC diatoms, particularly *C. dictyota*,  
628 with important implications for the strength of the biological carbon pump and transfer to higher trophic levels in  
629 these areas. Compared to the neritic diatoms of the more productive coastal areas, *C. dictyota* is a slow growing  
630 species, but within the diatoms characteristic of the HNLC areas it is among the faster growing ones, responding  
631 strongly to artificial (and natural) iron fertilization and contributing to carbon export. Thus, within this group, *C.*  
632 *dictyota* can be characterized as a bloom-former and carbon sinker.

633 It is important to note that while the main groups of the phytoplankton community were revealed by the pigment  
634 data, the resolution of pigment data is not high enough to differentiate between, for instance, different diatoms  
635 and delineate the patterns discussed above. Therefore, microscopy data or other imaging techniques are needed  
636 to determine microphytoplankton to species level in order to fully understand the community composition. It is  
637 also noteworthy that the pigment approach may not capture a large part of the dinoflagellate community with a  
638 peridinin-based pigment type, as in our study the majority of dinoflagellates belonged to the genus  
639 *Gymnodinium*, which contains similar pigments to e.g. diatoms and haptophytes and no peridinin (Jeffrey et al.,  
640 2011). In addition, non-pigment containing heterotrophic species call for different approaches to identify this  
641 important group. Finally, the haptophyte-type pigment group requires other types of analyses to be properly



642 identified. A possible solution for future studies could be a combination with 18S rRNA-sequencing, for a better  
643 interpretation of the various target groups.

644 This is the first thorough characterization of phytoplankton community composition in the area, studying the  
645 early autumn season. Future studies will show how it relates to the different seasons such as the early bloom  
646 phase in spring and whether seasonal succession can be seen in the community composition. In addition, the  
647 very near coast and coastal polynyas could not be sampled during this study and could potentially differ in their  
648 community composition, and future sampling can offer further insights into possible north-south gradients.

#### 649 **6. Data availability**

650 The data presented in this study can be found in online repositories (Norwegian Polar Data Centre,  
651 data.npolar.no) in Moreau et al. (2020) and Kauko et al. (2022).

#### 652 **7. Author contributions**

653 HMK planned the study, analysed the data and wrote the first manuscript draft. SM, HMK, TRK and AS planned  
654 and carried out the field work. HMK and AS analysed the FCM samples. PA contributed with expert knowledge.  
655 IP processed the pigment samples data and guided on the CHEMTAX analysis. MR and JW analysed the  
656 microscopy samples. GB arranged the FCM analysis and processed the data. All authors contributed to the  
657 manuscript writing.

#### 658 **8. Competing interest**

659 The authors declare that they have no conflict of interest.

#### 660 **9. Acknowledgements**

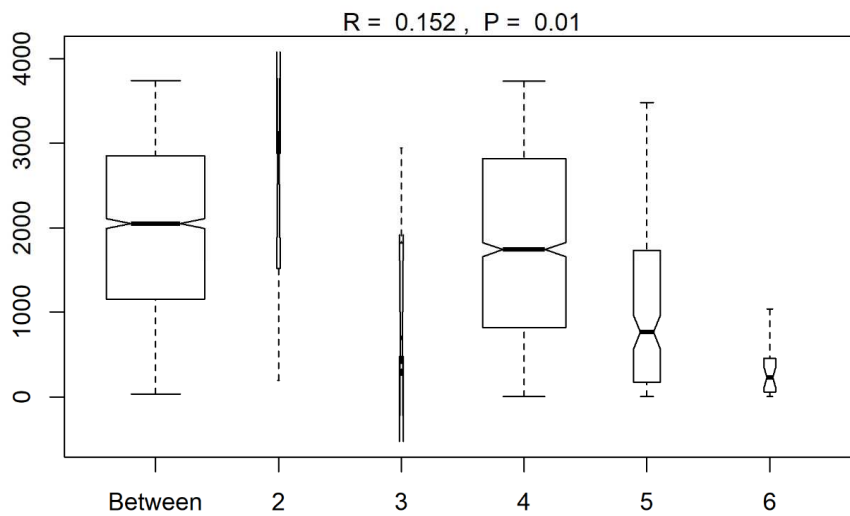
661 The Southern Ocean Ecosystem cruise 2019 was led by the Norwegian Polar Institute, with further financial  
662 support from the Norwegian Ministry of Foreign Affairs. The Research Council of Norway (grant number  
663 288370) and National Research Foundation, South Africa (grant UID 118715) project in the SANOCEAN  
664 Norway–South Africa collaboration contributed to this study.

665 We are thankful to the captain and crew of the RV Kronprins Haakon, Nadine Steiger and John Olav Vinge for  
666 help with water sampling, Elzbieta Anna Petelenz for supervising the flow cytometry measurements and Sandra  
667 Murawski and Lea Phillips for technical assistance with the HPLC measurements.



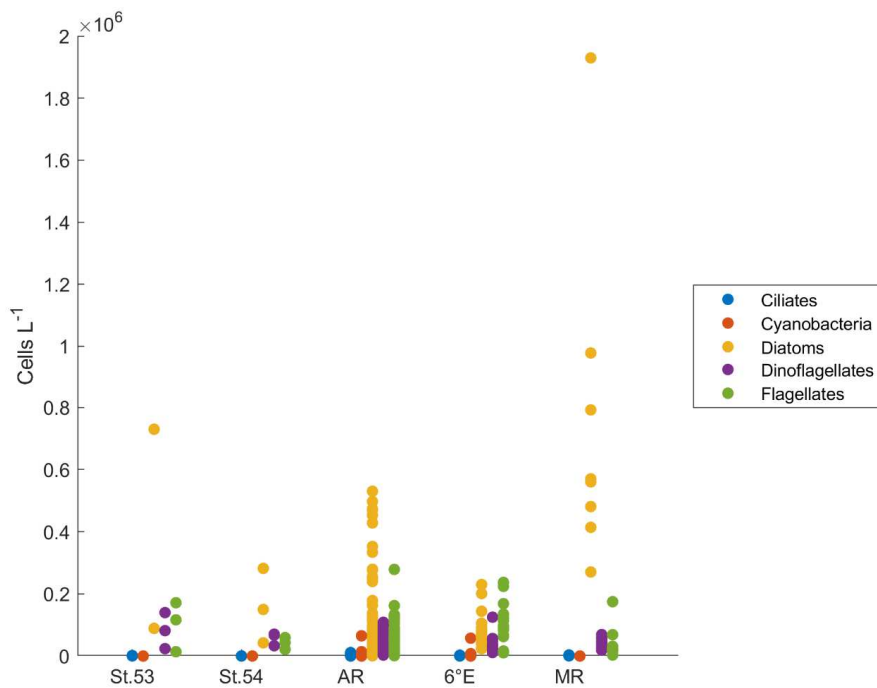
668 **10. Appendices**

669 **Appendix A. Supplementary figures.**



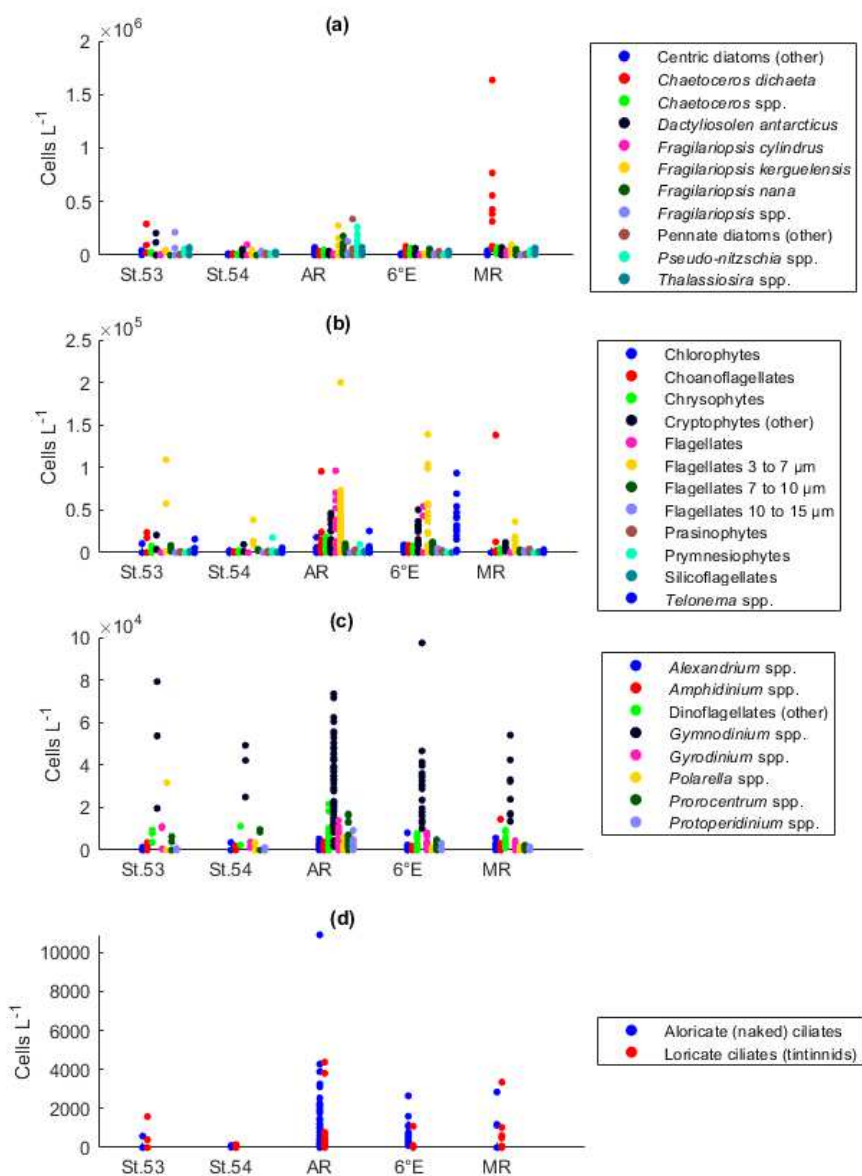
670

671 **Figure A1: A summary plot from the *anosim* analysis (testing differences between the sampling areas in species**  
672 **abundances after the NMDS analysis). Range of dissimilarities in the different areas (2-6: station 53, station 54, Astrid**  
673 **Ridge, the 6° E transect and Maud Rise, respectively).**



674

675 **Figure A2: Protist abundance in all samples in the different sampling areas based on microscopy. St.53=station 53,**  
676 **St.54=station 54, AR=Astrid Ridge, 6°E= 6° E transect, MR=Maud Rise.**



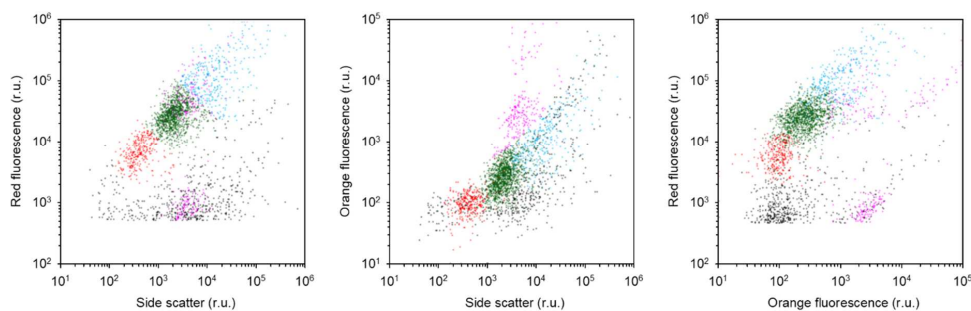
677

678 **Figure A3: Protist abundance in all samples in the different sampling areas (based on microscopy) for (a) diatoms, (b)**  
 679 **flagellates, (c) dinoflagellates and (d) ciliates. St.53=station 53, St.54=station 54, AR=Astrid Ridge, 6°E= 6° E transect,**  
 680 **MR=Maud Rise.**



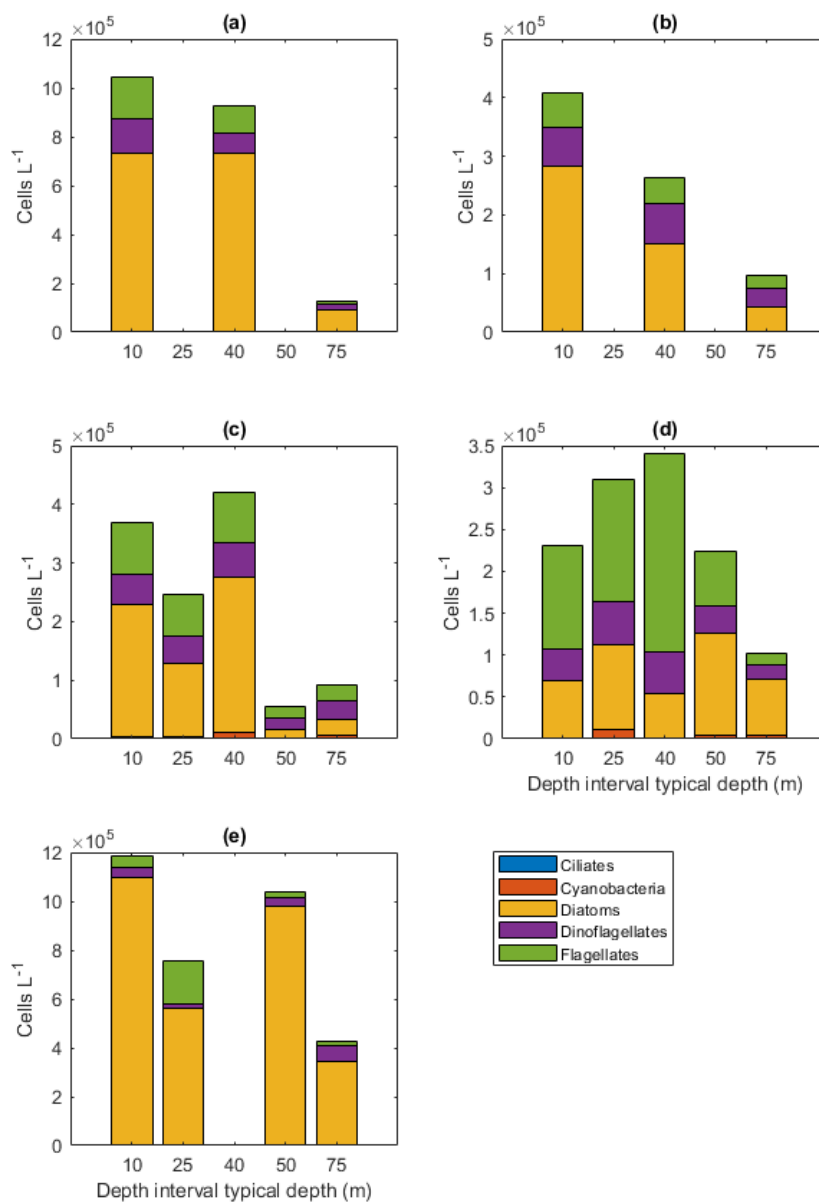
681

682 **Figure A4: Filamentous blue-green algae cf. *Anabaena* sp..**



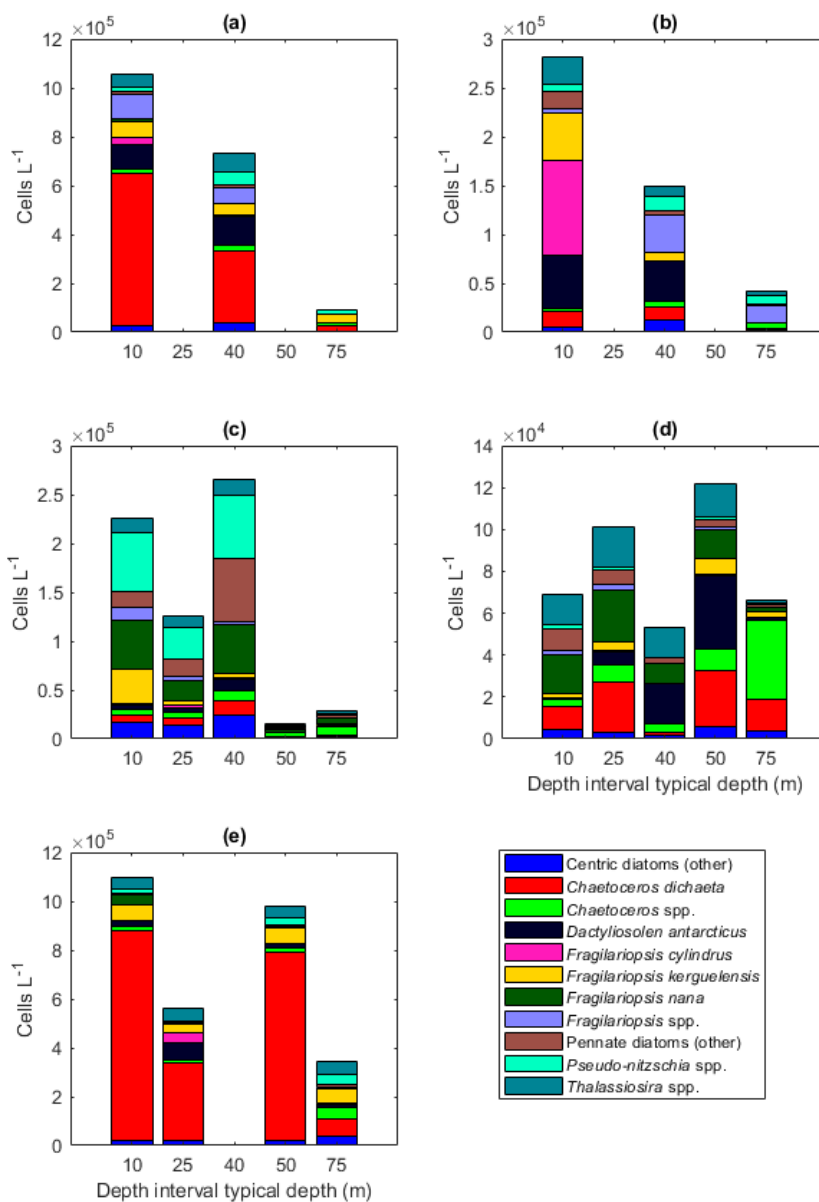
683

684 **Figure A5: Scatter plots indicating the position of the different phytoplankton populations in the cytograms.**  
685 **Picophytoplankton, Nanophytoplankton 1 and Nanophytoplankton 2 were discriminated based on chlorophyll red**  
686 **autofluorescence versus side scatter (red, green and blue dots respectively). Possible cyanobacteria and cryptophytes**  
687 **were in addition recognized based on their orange autofluorescence (violet dots). The example shown is from CTD**  
688 **station 61 at 40 m depth. Axis are in relative units (r.u.).**



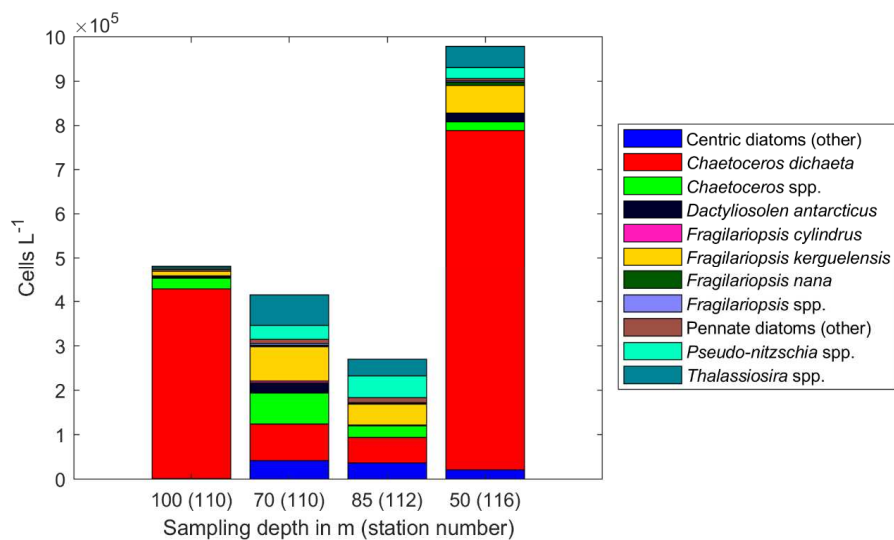
689

690 **Figure A6: Protist abundances in the different sampling areas averaged per depth interval for (a) station 53, (b)**  
 691 **station 54, (c) Astrid Ridge, (d) 6° E transect and (e) Maud Rise. Depth intervals (with typical sampling depth in**  
 692 **brackets): 5-10 (10); 25-35 (25), 35-45 (40), 50-60, 65-85 (75) m.**



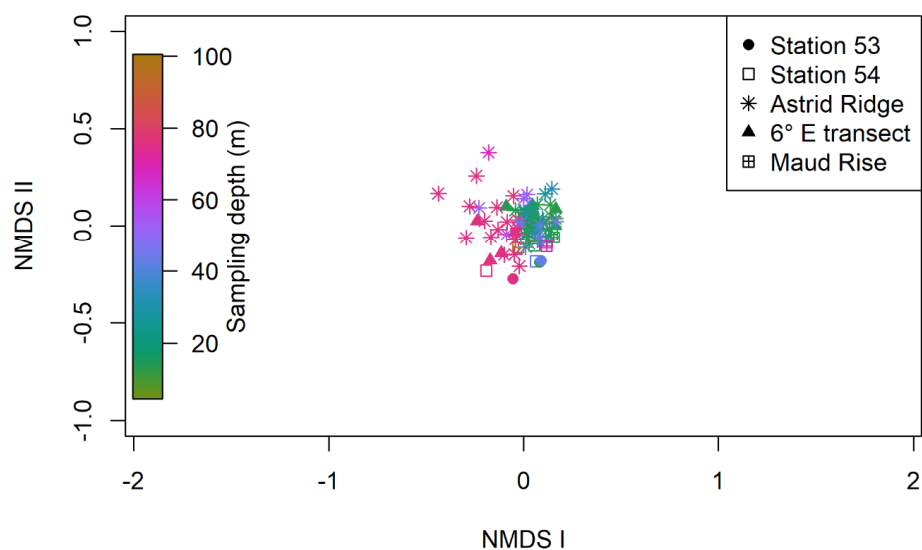
693

694 **Figure A7: Diatom abundance in the different sampling areas averaged per depth interval for (a) station 53, (b)**  
 695 **station 54, (c) Astrid Ridge, (d) 6° E transect and (e) Maud Rise. Depth intervals (with typical sampling depth in**  
 696 **brackets): 5-10 (10); 25-35 (25), 35-45 (40), 50-60, 65-85 (75) m.**



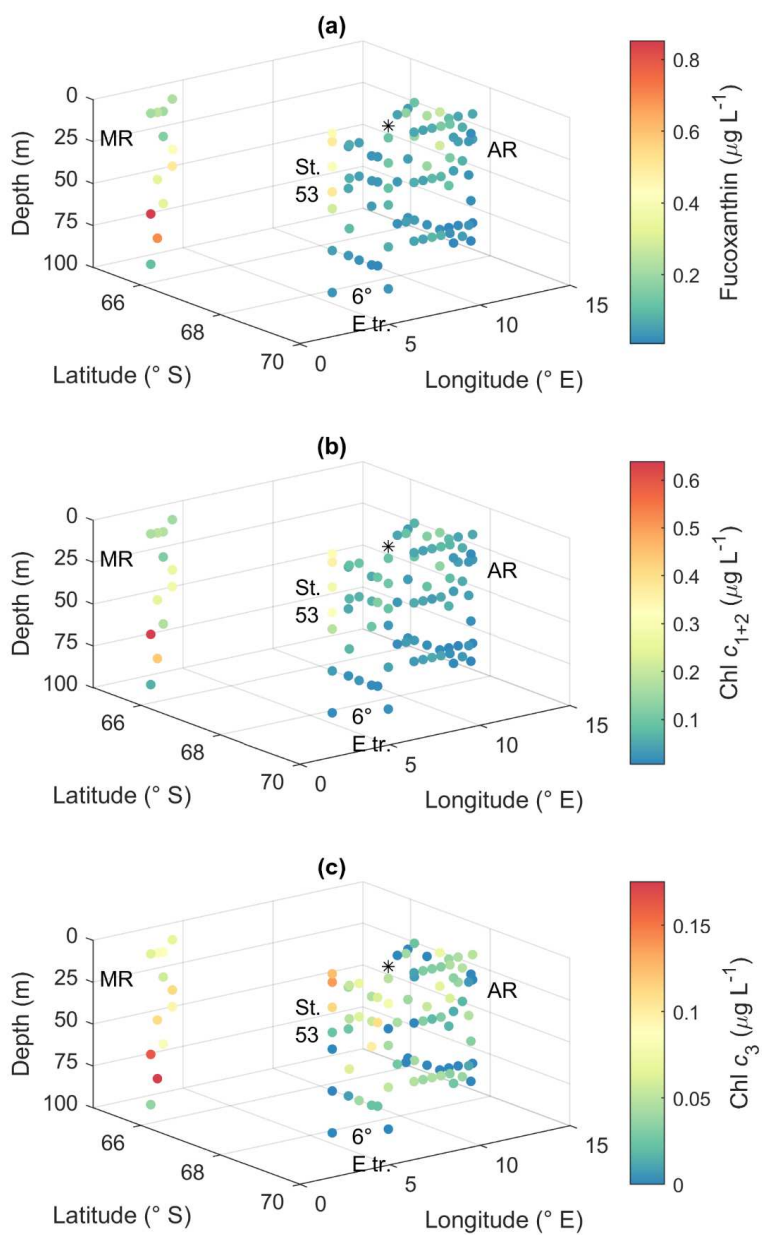
697

698 **Figure A8:** Diatom abundance in available deep samples at Maud Rise. Bars are marked with the sampling depth in  
 699 meters and the station number in brackets.



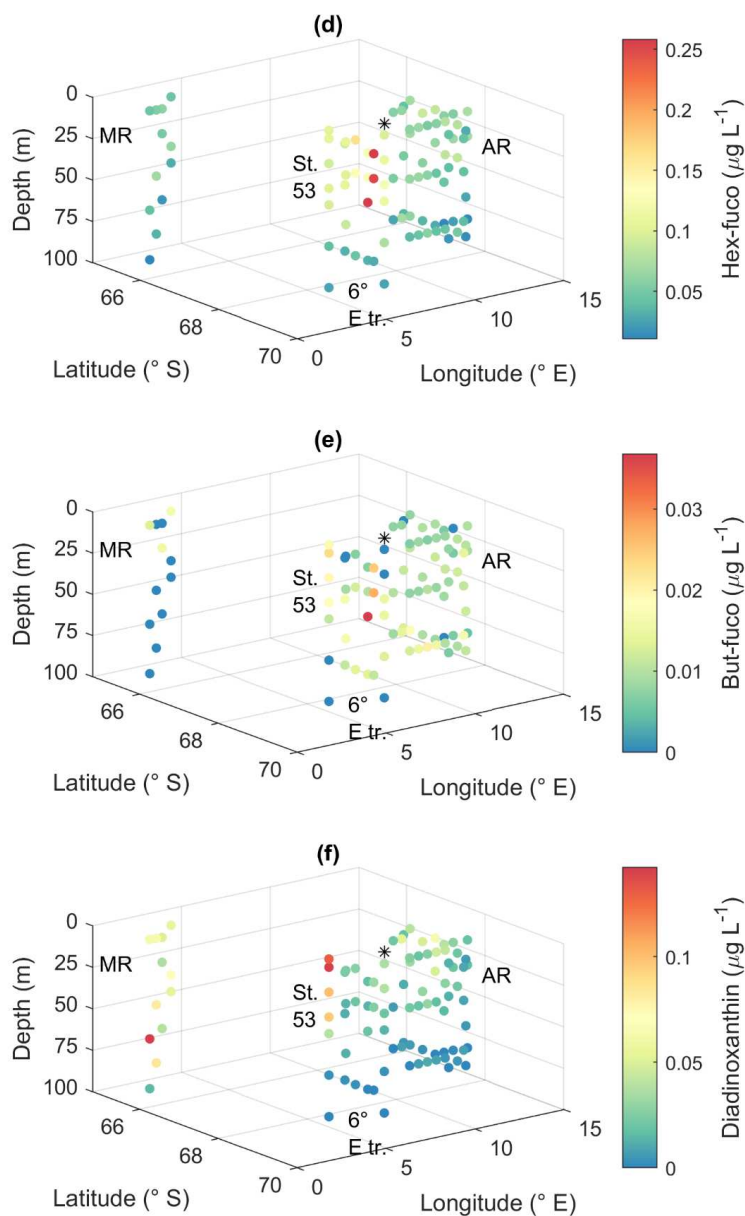
700

701 **Figure A9:** NMDS clustering using presence-absence data.



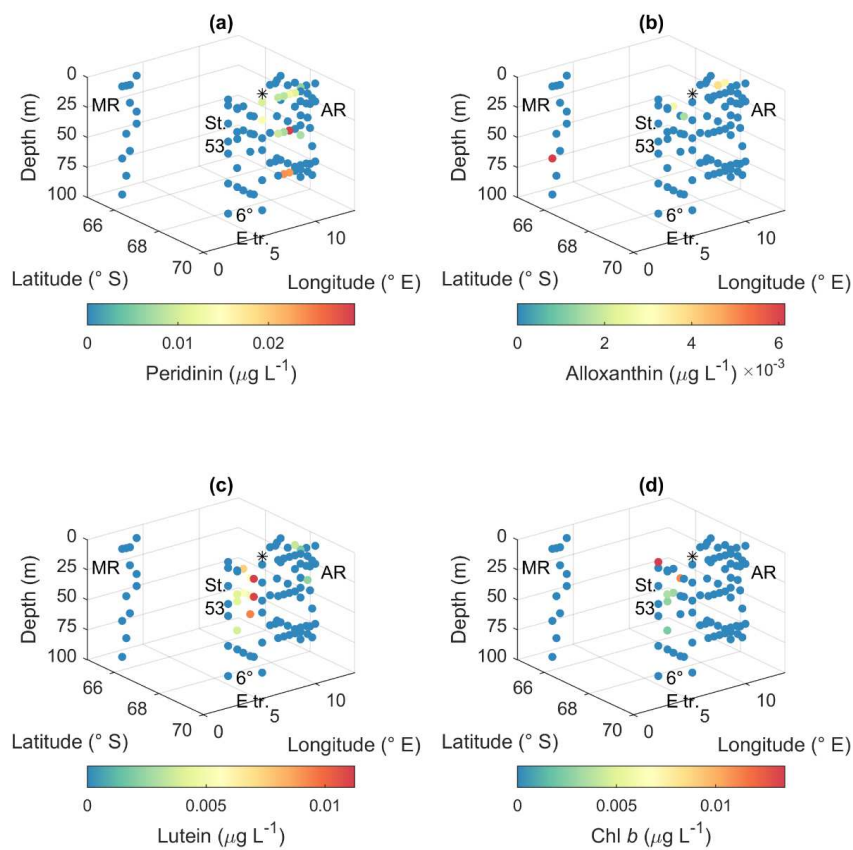
702

703



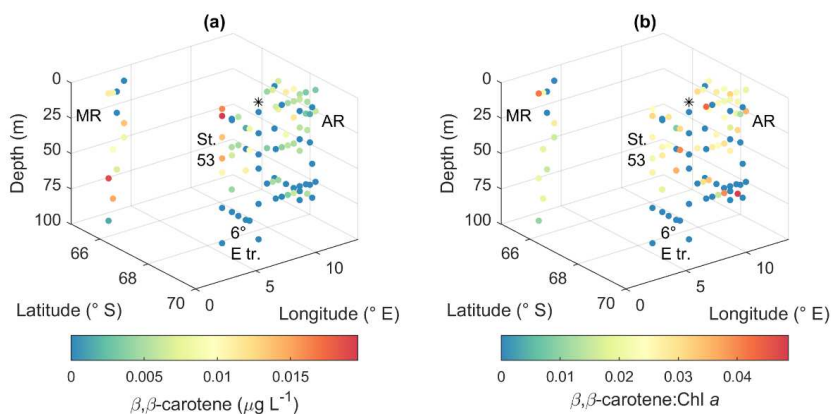
704

705 **Figure A10: Pigment concentrations of (a) fucoxanthin, (b) Chl  $c_{1+2}$ , (c) Chl  $c_3$ , (d) hex-fuco, (e) but-fuco and (f)**  
706 **diadinoxanthin. MR=Maud Rise, St. 53=station 53, AR=Astrid Ridge, 6° E tr.= 6° E transect. Station 54 is marked**  
707 **with a black asterisk.**



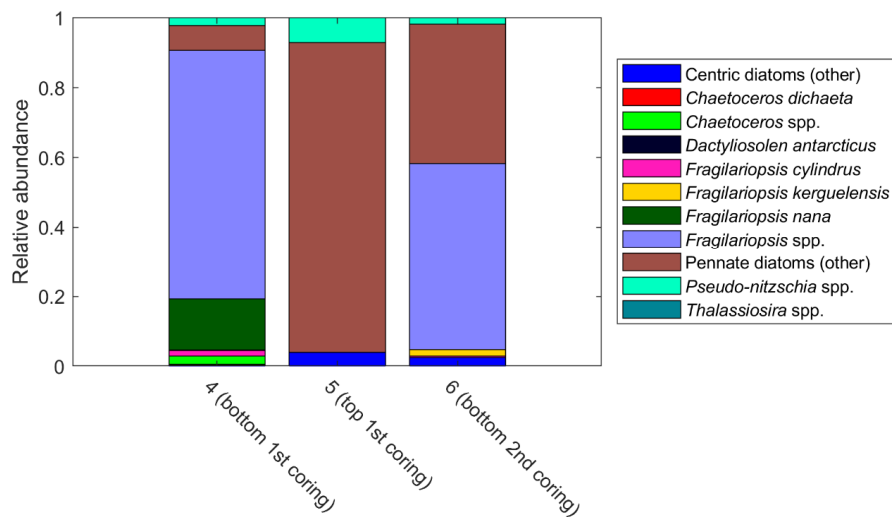
708

709 **Figure A11: Pigment concentrations of (a) peridinin, (b) alloxanthin, (c) lutein and (d) Chl *b*.** MR=Maud Rise, St.  
710 53=station 53, AR=Astrid Ridge, 6° E tr.= 6° E transect. Station 54 is marked with a black asterisk.



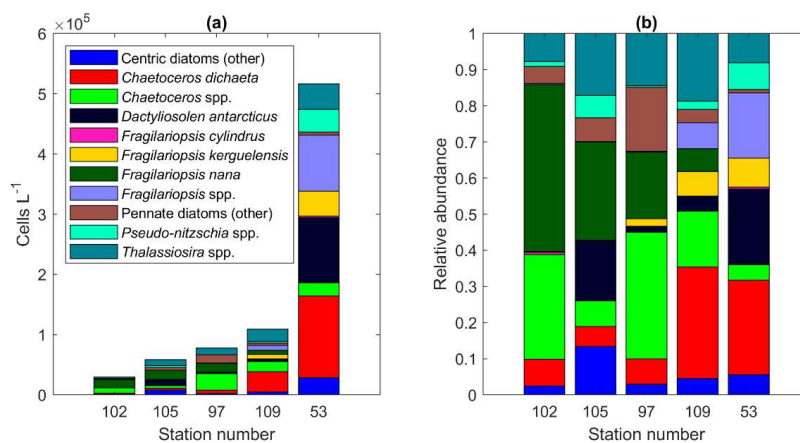
711

712 **Figure A12:** (a)  $\beta, \beta$ -carotene concentration and (b) ratio of  $\beta, \beta$ -carotene to Chl a. MR=Maud Rise, St. 53=station 53,  
 713 AR=Astrid Ridge, 6° E tr.= 6° E transect. Station 54 is marked with a black asterisk.



714

715 **Figure A13:** Relative diatom abundance in ice core samples. The colours pink to cyan comprise pennate diatoms. The  
 716 bars are marked with sample numbers and ice core section explanations. See Table B2 for method descriptions.



717

718 **Figure A14: (a) Diatom abundance and (b) relative abundance in the south-north transect at 6° E including the**  
 719 **station 53 just north of the transect (average abundances per station).**



720 **Appendix B. Supplementary tables.**

721 **Table B1.** All taxa identified in the CTD station samples down to 100 m (in total 87 samples). For median abundance 2, only the samples where the species/taxon was  
 722 observed were taken into account (i.e., zero abundances do not contribute to the median value).

Class/group	Species/taxon	Number of samples observed in	Median abundance 1 (cells L <sup>-1</sup> )	Median abundance 2 (cells L <sup>-1</sup> )	Station 53	Station 54	Astrid Ridge	6° E transect	Maud Rise
Bacillariophyceae	<i>Actinocyclus</i> sp.	1	0	2411			x		
Bacillariophyceae	<i>Actinocyclus actinochilus</i>	19	0	95	x		x	x	x
Bacillariophyceae	<i>Actinocyclus curvatulus</i>	3	0	1404			x		x
Bacillariophyceae	<i>Asteromphalus</i> spp.	34	0	293			x	x	x
Bacillariophyceae	<i>Asteromphalus hyalinus</i>	51	297	2119	x	x	x	x	x
Bacillariophyceae	<i>Asteromphalus parvulus</i>	50	302	1113	x	x	x	x	x
Bacillariophyceae	<i>Auricula compacta</i>	7	0	378			x		x
Bacillariophyceae	<i>Banquisia belgicae</i>	36	0	373	x		x	x	x
Bacillariophyceae	<i>Chaetoceros</i> spp.	55	1261	4558	x	x	x	x	x
Bacillariophyceae	<i>Chaetoceros affinis</i>	1	0	7798			x		
Bacillariophyceae	<i>Chaetoceros atlanticus</i>	33	0	866	x	x	x	x	x
Bacillariophyceae	<i>Chaetoceros atlanticus f. bulbosus</i>	42	0	510	x		x	x	x
Bacillariophyceae	<i>Chaetoceros bulbosus</i>	32	0	213	x	x	x	x	x
Bacillariophyceae	<i>Chaetoceros castracanei</i>	50	151	368			x	x	x
Bacillariophyceae	<i>Chaetoceros concavicornis</i>	1	0	2133			x		
Bacillariophyceae	<i>Chaetoceros convolutus</i>	1	0	3562	x				
Bacillariophyceae	<i>Chaetoceros cryophilus</i>	3	0	830			x		x
Bacillariophyceae	<i>Chaetoceros curvatus</i>	41	0	257		x	x	x	x
Bacillariophyceae	<i>Chaetoceros decipiens</i>	1	0	3059	x				





Bacillariophyceae	<i>Haslea trompii</i>	1	0	1664				x		
Bacillariophyceae	<i>Haslea vitrea</i>	2	0	354						x
Bacillariophyceae	<i>Leptocylindrus mediterraneus</i>	33	0	195	x			x		x
Bacillariophyceae	<i>Membraneis challengeri</i>	25	0	396	x	x		x		x
Bacillariophyceae	<i>Navicula</i> spp.	60	179	399	x	x		x		x
Bacillariophyceae	<i>Navicula criophila</i>	1	0	1583	x					
Bacillariophyceae	<i>Navicula directa</i> var. <i>directa</i>	1	0	86				x		
Bacillariophyceae	<i>Navicula transitans</i>	1	0	109				x		
Bacillariophyceae	<i>Nitzschia longissima</i>	41	0	333				x	x	x
Bacillariophyceae	<i>Odontella</i> sp.	1	0	778				x		
Bacillariophyceae	<i>Odontella weissflogii</i>	1	0	176				x		
Bacillariophyceae	Pennales	59	302	757		x		x	x	x
Bacillariophyceae	Phaeoceros	4	0	516	x			x	x	
Bacillariophyceae	<i>Plagiotropus gausсии</i>	1	0	938				x		
Bacillariophyceae	<i>Proboscia</i> spp.	12	0	221	x			x		x
Bacillariophyceae	<i>Proboscia alata</i>	61	169	378	x	x		x	x	x
Bacillariophyceae	<i>Proboscia inermis</i>	29	0	172	x	x		x	x	x
Bacillariophyceae	<i>Proboscia truncata</i>	6	0	315				x		
Bacillariophyceae	<i>Pseudo-nitzschia</i> spp.	78	1474	1887	x	x		x	x	x
Bacillariophyceae	<i>Pseudo-nitzschia heimii</i>	28	0	3392	x	x		x	x	
Bacillariophyceae	<i>Pseudo-nitzschia lineola</i>	13	0	1245	x	x		x	x	
Bacillariophyceae	<i>Pseudo-nitzschia turgidula</i>	1	0	1105				x		
Bacillariophyceae	<i>Pseudo-nitzschia turgiduloides</i>	1	0	2010				x		
Bacillariophyceae	<i>Rhizolenia</i> spp.	25	0	165	x	x		x	x	x
Bacillariophyceae	<i>Rhizolenia delicatula</i>	1	0	792	x					
Bacillariophyceae	<i>Rhizolenia hebetata</i>	3	0	396	x			x		
Bacillariophyceae	<i>Rhizolenia hebetata</i> f. <i>semispina</i>	19	0	137	x	x		x	x	x
Bacillariophyceae	<i>Rhizolenia imbricata</i>	25	0	218	x	x		x	x	x
Bacillariophyceae	<i>Rhizolenia simplex</i>	2	0	534				x		











725 **Table B2.** Comparison of the 20 most abundant diatom species between sea ice samples and Astrid Ridge  
 726 samples. Green colour indicates presence in both areas.

Ice samples (most abundant diatoms)	Average abundance (all samples; cells L <sup>-1</sup> )	Astrid Ridge (most abundant diatoms)	Average abundance (samples down to 100 m; cells L <sup>-1</sup> )
<i>Fragilariopsis</i> spp.	782601	<i>Pseudo-nitzschia</i> spp.	30105
<i>Fragilariopsis nana</i>	152180	<i>Fragilariopsis nana</i>	27081
<i>Cylindrotheca closterium</i>	53846	<i>Fragilariopsis kerguelensis</i>	13004
<i>Pseudo-nitzschia</i> spp.	25263	<i>Thalassiosira</i> spp.	8164
<i>Eucampia antarctica</i>	21718	<i>Thalassiothrix antarctica</i>	6068
<i>Chaetoceros</i> spp.	19298	<i>Chaetoceros dicaeta</i>	5954
<i>Fragilariopsis cylindrus</i>	16473	<i>Dactyliosolen tenuijunctus</i>	5823
<i>Haslea</i> spp.	11706	<i>Cylindrotheca closterium</i>	4436
<i>Synedropsis</i> spp.	9547	<i>Fragilariopsis</i> spp.	4389
Pennales	7604	<i>Dactyliosolen antarcticus</i>	3731
<i>Navicula</i> spp.	4949	<i>Chaetoceros</i> spp.	3164
<i>Chaetoceros socialis</i>	4365	Pennales	1656
<i>Entomoneis paludosa</i>	3201	<i>Haslea</i> spp.	1646
<i>Fragilariopsis kerguelensis</i>	2855	<i>Synedropsis</i> spp.	1330
<i>Dactyliosolen tenuijunctus</i>	2828	<i>Asteromphalus hyalinus</i>	1269
<i>Banquisia belgicae</i>	2466	<i>Fragilariopsis cylindrus</i>	1267
<i>Chaetoceros curvatus</i>	2341	<i>Corethron pennatum</i>	1235
<i>Fragilariopsis rhombica</i>	2341	<i>Pseudo-nitzschia heimii</i>	1199
<i>Corethron pennatum</i>	2328	<i>Pseudo-nitzschia lineola</i>	1133
<i>Odontella</i> spp.	1540	<i>Thalassiosira gracilis</i>	1113

727

728 Two ice floes were sampled along the 6° E transect (the first one on 26.3.2019 at 68.9135° S and 6.0217° E, and  
 729 the second one on 27.3.2019 at 68.4392° S and 5.9135° E). Ice algal taxonomy and abundance samples were  
 730 taken from in total 3 ice core sections: a 10 cm bottom section and an 8.5 cm top section from the 18.5 cm thick  
 731 ice core at the first ice floe, and a 10 cm bottom section from the 93,5 cm thick ice core at the second ice floe. A  
 732 Kovacs 9 cm corer was used, and the ice samples were melted without the addition of filtered sea water in  
 733 darkness and room temperature, and processed as soon as the melting was complete.

734



735 **11. References**

- 736 Abelmann, A., Gersonde, R., Cortese, G., Kuhn, G. and Smetacek, V.: Extensive phytoplankton blooms in the  
737 Atlantic sector of the glacial Southern Ocean, *Paleoceanography*, 21, PA1013, doi:10.1029/2005PA001199,  
738 2006.
- 739 Anderson, M. J. and Walsh, D. C. I.: PERMANOVA, ANOSIM, and the Mantel test in the face of  
740 heterogeneous dispersions: What null hypothesis are you testing?, *Ecol. Monogr.*, 83(4), 557–574,  
741 doi:10.1890/12-2010.1, 2013.
- 742 Armand, L. K., Cornet-Barthaux, V., Mosseri, J. and Quéguiner, B.: Late summer diatom biomass and  
743 community structure on and around the naturally iron-fertilised Kerguelen Plateau in the Southern Ocean, *Deep*  
744 *Res. Part II Top. Stud. Oceanogr.*, 55(5–7), 653–676, doi:10.1016/j.dsr2.2007.12.031, 2008.
- 745 Arrigo, K. R. and van Dijken, G. L.: Phytoplankton dynamics within 37 Antarctic coastal polynya systems, *J.*  
746 *Geophys. Res.*, 108(8), C83271, doi:10.1029/2002jc001739, 2003.
- 747 Arrigo, K. R., Robinson, D. H., Worthen, D. L., Dunbar, R. B., DiTullio, G. R., VanWoert, M. and Lizotte, M.  
748 P.: Phytoplankton community structure and the drawdown of nutrients and CO<sup>2</sup> in the Southern Ocean, *Science.*,  
749 283(5400), 365–367, doi:10.1126/science.283.5400.365, 1999.
- 750 Assmy, P., Hernández-Becerril, D. U. and Montresor, M.: Morphological variability and life cycle traits of the  
751 type species of the diatom genus *Chaetoceros*, *C. dictyota*, *J. Phycol.*, 44(1), 152–163, doi:10.1111/j.1529-  
752 8817.2007.00430.x, 2008.
- 753 Assmy, P., Smetacek, V., Montresor, M., Klaas, C., Henjes, J., Strass, V. H., Arrieta, J. M., Bathmann, U., Berg,  
754 G. M., Breitbarth, E., Cisewski, B., Friedrichs, L., Fuchs, N., Herndl, G. J., Jansen, S., Krägersky, S., Latasa, M.,  
755 Peeken, I., Röttgers, R., Scharek, R., Schüller, S. E., Steigenberger, S., Webb, A. and Wolf-Gladrow, D.: Thick-  
756 shelled, grazer-protected diatoms decouple ocean carbon and silicon cycles in the iron-limited Antarctic  
757 Circumpolar Current, *Proc. Natl. Acad. Sci. U. S. A.*, 110(51), 20633–20638, doi:10.1073/pnas.1309345110,  
758 2013.
- 759 Balch, W. M., Bates, N. R., Lam, P. J., Twining, B. S., Rosengard, S. Z., Bowler, B. C., Drapeau, D. T., Garley,  
760 R., Lubelczyk, L. C., Mitchell, C. and Rauschenberg, S.: Factors regulating the Great Calcite Belt in the  
761 Southern Ocean and its biogeochemical significance, *Global Biogeochem. Cycles*, 30, 1199–1214,  
762 doi:10.1002/2016GB005414, 2016.
- 763 Baldry, K., Stratton, P. G., Hill, N. A. and Boyd, P. W.: Subsurface chlorophyll-a maxima in the Southern  
764 Ocean, *Front. Mar. Sci.*, 7, 671, doi:10.3389/fmars.2020.00671, 2020.
- 765 Bendif, E. M., Nevado, B., Wong, E. L. Y., Hagino, K., Probert, I., Young, J. R., Rickaby, R. E. M. and Filatov,  
766 D. A.: Repeated species radiations in the recent evolution of the key marine phytoplankton lineage  
767 *Gephyrocapsa*, *Nat. Commun.*, 10, 4234, doi:10.1038/s41467-019-12169-7, 2019.
- 768 von Berg, L., Prend, C. J., Campbell, E. C., Mazloff, M. R., Talley, L. D. and Gille, S. T.: Weddell Sea  
769 phytoplankton blooms modulated by sea ice variability and polynya formation, *Geophys. Res. Lett.*, 47,



- 770 e2020GL087954, doi:10.1029/2020GL087954, 2020.
- 771 Blain, S., Quéguiner, B., Armand, L., Belviso, S., Bombléd, B., Bopp, L., Bowie, A., Brunet, C., Brussaard, C.,  
772 Carlotti, F., Christaki, U., Corbière, A., Durand, I., Ebersbach, F., Fuda, J. L., Garcia, N., Gerringa, L., Griffiths,  
773 B., Guigue, C., Guillerm, C., Jacquet, S., Jeandel, C., Laan, P., Lefèvre, D., Lo Monaco, C., Malits, A., Mosseri,  
774 J., Obernosterer, I., Park, Y. H., Picheral, M., Pondaven, P., Remenyi, T., Sandroni, V., Sarthou, G., Savoye, N.,  
775 Scouarnec, L., Souhaut, M., Thuiller, D., Timmermans, K., Trull, T., Uitz, J., Van Beek, P., Veldhuis, M.,  
776 Vincent, D., Viollier, E., Vong, L. and Wagener, T.: Effect of natural iron fertilization on carbon sequestration in  
777 the Southern Ocean, *Nature*, 446(7139), 1070–1074, doi:10.1038/nature05700, 2007.
- 778 Buma, A. G. J., Treguer, P., Kraaij, G. W. and Morvan, J.: Algal pigment patterns in different watermasses of  
779 the Atlantic sector of the Southern Ocean during fall 1987, *Polar Biol.*, 11(1), 55–62, doi:10.1007/BF00236522,  
780 1990.
- 781 Coale, K. H., Johnson, K. S., Chavez, F. P., Buesseler, K. O., Barber, R. T., Brzezinski, M. A., Cochlan, W. P.,  
782 Millero, F. J., Falkowski, P. G., Bauer, J. E., Wanninkhof, R. H., Kudela, R. M., Altabet, M. A., Hales, B. E.,  
783 Takahashi, T., Landry, M. R., Bidigare, R. R., Wang, X., Chase, Z., Strutton, P. G., Friederich, G. E., Gorbunov,  
784 M. Y., Lance, V. P., Hiltling, A. K., Hiscock, M. R., Demarest, M., Hiscock, W. T., Sullivan, K. F., Tanner, S. J.,  
785 Gordon, R. M., Hunter, C. N., Elrod, V. A., Fitzwater, S. E., Jones, J. L., Tozzi, S., Koblizek, M., Roberts, A. E.,  
786 Herndon, J., Brewster, J., Ladizinsky, N., Smith, G., Cooper, D., Timothy, D., Brown, S. L., Selph, K. E.,  
787 Sheridan, C. C., Twining, B. S. and Johnson, Z. I.: Southern Ocean iron enrichment experiment: carbon cycling  
788 in high- and low-Si waters, *Science*, 304(5669), 408–414, doi:10.1126/science.1089778, 2004.
- 789 Davidson, A. T., Scott, F. J., Nash, G. V., Wright, S. W. and Raymond, B.: Physical and biological control of  
790 protistan community composition, distribution and abundance in the seasonal ice zone of the Southern Ocean  
791 between 30 and 80°E, *Deep. Res. Part II Top. Stud. Oceanogr.*, 57(9–10), 828–848,  
792 doi:10.1016/j.dsr2.2009.02.011, 2010.
- 793 Deppeler, S. L. and Davidson, A. T.: Southern Ocean phytoplankton in a changing climate, *Front. Mar. Sci.*, 4,  
794 40, doi:10.3389/fmars.2017.00040, 2017.
- 795 Detmer, A. E. and Bathmann, U. V.: Distribution patterns of autotrophic pico- and nanoplankton and their  
796 relative contribution to algal biomass during spring in the Atlantic sector of the Southern Ocean, *Deep. Res. Part*  
797 *II Top. Stud. Oceanogr.*, 44(1–2), 299–320, doi:10.1016/S0967-0645(96)00068-9, 1997.
- 798 Dinniman, M. S., St-Laurent, P., Arrigo, K. R., Hofmann, E. E. and van Dijken, G. L.: Analysis of iron sources  
799 in Antarctic Continental Shelf waters, *J. Geophys. Res. Ocean.*, 125(5), e2019JC015736,  
800 doi:10.1029/2019JC015736, 2020.
- 801 Dong, J., Speer, K. and Jullion, L.: The Antarctic Slope Current near 30° E, *J. Geophys. Res. Ocean.*, 121, 1051–  
802 1062, doi:10.1038/175238c0, 2016.
- 803 Edler, L. and Elbrächter, M.: The Utermöhl method for quantitative phytoplankton analysis, in *Microscopic and*  
804 *Molecular Methods for Quantative Phytoplankton analysis*, edited by B. Karlson, C. Cusack, and E. Bresnan, pp.  
805 13–20, Intergovernmental Oceanographic Commission of UNESCO, Paris., 2010.



- 806 Gibberd, M. J., Kean, E., Barlow, R., Thomalla, S. and Lucas, M.: Phytoplankton chemotaxonomy in the  
807 Atlantic sector of the Southern Ocean during late summer 2009, *Deep. Res. Part I Oceanogr. Res. Pap.*, 78, 70–  
808 78, doi:10.1016/j.dsr.2013.04.007, 2013.
- 809 Gomi, Y., Fukuchi, M. and Taniguchi, A.: Diatom assemblages at subsurface chlorophyll maximum layer in the  
810 eastern Indian sector of the Southern Ocean in summer, *J. Plankton Res.*, 32(7), 1039–1050,  
811 doi:10.1093/plankt/fbq031, 2010.
- 812 Granéli, E., Granéli, W., Rabbani, M. M., Daugbjerg, N., Fransz, G., Roudy, J. C. and Alder, V. A.: The  
813 influence of copepod and krill grazing on the species composition of phytoplankton communities from the Scotia  
814 Weddell sea - An experimental approach, *Polar Biol.*, 13(3), 201–213, doi:10.1007/BF00238930, 1993.
- 815 Hansen, B., Bjornsen, P. K. and Hansen, P. J.: The size ratio between planktonic predators and their prey,  
816 *Limnol. Oceanogr.*, 39(2), 395–403, doi:10.4319/lo.1994.39.2.0395, 1994.
- 817 Hardge, K., Peeken, I., Neuhaus, S., Lange, B. A., Stock, A., Stoeck, T., Weinsich, L. and Metfies, K.: The  
818 importance of sea ice for exchange of habitat-specific protist communities in the Central Arctic Ocean, *J. Mar.*  
819 *Syst.*, 165, 124–138, doi:10.1016/j.jmarsys.2016.10.004, 2017.
- 820 Higgins, H. W., Wright, S. W. and Schlüter, L.: Quantative interpretation of chemotaxonomic pigment data, in  
821 *Phytoplankton Pigments - Characterization, Chemotaxonomy and Applications in Oceanography*, edited by S.  
822 Roy, C. A. LLewellyn, E. S. Egeland, and G. Johnsen, pp. 257–313, Cambridge University Press, New York.,  
823 2011.
- 824 Hop, H., Vihtakari, M., Bluhm, B. A., Assmy, P., Poulin, M., Gradinger, R., Peeken, I., von Quillfeldt, C.,  
825 Olsen, L. M., Zhitina, L. and Melnikov, I. A.: Changes in sea-ice protist diversity with declining sea ice in the  
826 Arctic Ocean from the 1980s to 2010s, *Front. Mar. Sci.*, 7, 243, doi:10.3389/fmars.2020.00243, 2020.
- 827 Irigoien, X., Hulsman, J. and Harris, R. P.: Global biodiversity patterns of marine phytoplankton and  
828 zooplankton, *Nature*, 429(6994), 863–867, doi:10.1038/nature02593, 2004.
- 829 Irigoien, X., Flynn, K. J. and Harris, R. P.: Phytoplankton blooms: A “loophole” in microzooplankton grazing  
830 impact?, *J. Plankton Res.*, 27(4), 313–321, doi:10.1093/plankt/fbi011, 2005.
- 831 Jeffrey, S. W., Wright, S. W. and Zapata, M.: Microalgal classes and their signature pigments, in *Phytoplankton*  
832 *Pigments - Characterization, Chemotaxonomy and Applications in Oceanography*, edited by S. Roy, C. A.  
833 LLewellyn, E. S. Egeland, and G. Johnsen, pp. 3–77, Cambridge University Press, Cambridge., 2011.
- 834 Jena, B. and Pillai, A. N.: Satellite observations of unprecedented phytoplankton blooms in the Maud Rise  
835 polynya, Southern Ocean, *Cryosphere*, 14(4), 1385–1398, doi:10.5194/tc-14-1385-2020, 2020.
- 836 Kang, S. H. and Fryxell, G. A.: Phytoplankton in the Weddell Sea, Antarctica: composition, abundance and  
837 distribution in water-column assemblages of the marginal ice-edge zone during austral autumn, *Mar. Biol.*,  
838 116(2), 335–348, doi:10.1007/BF00350024, 1993.
- 839 Kauko, H. M., Olsen, L. M., Duarte, P., Peeken, I., Granskog, M. A., Johnsen, G., Fernández-Méndez, M.,  
840 Pavlov, A. K., Mundy, C. J. and Assmy, P.: Algal colonization of young Arctic sea ice in Spring, *Front. Mar.*



- 841 Sci., 5, 199, doi:10.3389/fmars.2018.00199, 2018.
- 842 Kauko, H. M., Moreau, S. and Hattermann, T.: Southern Ocean Ecosystem cruise 2019 vertical in situ  
843 chlorophyll a profiles [Data set], Norwegian Polar Institute, doi:10.21334/npolar.2021.5e510f85, 2020.
- 844 Kauko, H. M., Hattermann, T., Ryan-Keogh, T., Singh, A., de Steur, L., Fransson, A., Chierici, M., Falkenhaus,  
845 T., Hallfredsson, E. H., Bratbak, G., Tsagaraki, T., Berge, T., Zhou, Q. and Moreau, S.: Phenology and  
846 environmental control of phytoplankton blooms in the Kong Håkon VII Hav in the Southern Ocean, *Front. Mar.*  
847 *Sci.*, 8, 623856, doi:10.3389/fmars.2021.623856, 2021.
- 848 Kauko, H. M., Moreau, S., Rózańska, M. and Wiktor, J. M.: Southern Ocean Ecosystem cruise 2019  
849 phytoplankton taxonomy and abundance [Data set], Norwegian Polar Institute,  
850 doi:10.21334/npolar.2022.283e500c, 2022.
- 851 Kopczynska, E. E.: Dominance of microflagellates over diatoms in the Antarctic areas of deep vertical mixing  
852 and krill concentrations, *J. Plankton Res.*, 14(8), 1031–1054, doi:10.1093/plankt/14.8.1031, 1992.
- 853 Lasbleiz, M., Leblanc, K., Armand, L. K., Christaki, U., Georges, C., Obernosterer, I. and Quéguiner, B.:  
854 Composition of diatom communities and their contribution to plankton biomass in the naturally iron-fertilized  
855 region of Kerguelen in the Southern Ocean, *FEMS Microbiol. Ecol.*, 92(11), fiw171,  
856 doi:10.1093/femsec/fiw171, 2016.
- 857 van Leeuwe, M. A. and Stefels, J.: Effects of iron and light stress on the biochemical composition of Antarctic  
858 *Phaeocystis* sp. (Prymnesiophyceae). II. Pigment composition, *J. Phycol.*, 34(3), 496–503, doi:10.1046/j.1529-  
859 8817.1998.340486.x, 1998.
- 860 van Leeuwe, M. A., Kattner, G., van Oijen, T., de Jong, J. T. M. and de Baar, H. J. W.: Phytoplankton and  
861 pigment patterns across frontal zones in the Atlantic sector of the Southern Ocean, *Mar. Chem.*, 177, 510–517,  
862 doi:10.1016/j.marchem.2015.08.003, 2015.
- 863 van Leeuwe, M. A., Tedesco, L., Arrigo, K. R., Assmy, P., Campbell, K., Meiners, K. M., Rintala, J.-M., Selz,  
864 V., Thomas, D. N. and Stefels, J.: Microalgal community structure and primary production in Arctic and  
865 Antarctic sea ice: A synthesis, *Elem. Sci. Anthr.*, 6, 4, doi:10.1525/elementa.267, 2018.
- 866 van Leeuwe, M. A., Webb, A. L., Venables, H. J., Visser, R. J. W., Meredith, M. P., Elzenga, J. T. M. and  
867 Stefels, J.: Annual patterns in phytoplankton phenology in Antarctic coastal waters explained by environmental  
868 drivers, *Limnol. Oceanogr.*, 65(7), 1651–1668, doi:10.1002/lno.11477, 2020.
- 869 Leu, E., Mundy, C. J., Assmy, P., Campbell, K., Gabrielsen, T. M., Gosselin, M., Juul-Pedersen, T. and  
870 Gradinger, R.: Arctic spring awakening – Steering principles behind the phenology of vernal ice algal blooms,  
871 *Prog. Oceanogr.*, 139, 151–170, doi:10.1016/j.pocean.2015.07.012, 2015.
- 872 Löder, M. G. J., Meunier, C., Wiltshire, K. H., Boersma, M. and Aberle, N.: The role of ciliates, heterotrophic  
873 dinoflagellates and copepods in structuring spring plankton communities at Helgoland Roads, North Sea, *Mar.*  
874 *Biol.*, 158(7), 1551–1580, doi:10.1007/s00227-011-1670-2, 2011.
- 875 Mackey, M. D., Mackey, D. J., Higgins, H. W. and Wright, S. W.: CHEMTAX - A program for estimating class



- 876 abundances from chemical markers: Application to HPLC measurements of phytoplankton, *Mar. Ecol. Prog.*  
877 *Ser.*, 144(1–3), 265–283, doi:10.3354/meps144265, 1996.
- 878 Van den Meersche, K., Soetaert, K. and Middelburg, J. J.: A Bayesian compositional estimator for microbial  
879 taxonomy based on biomarkers, *Limnol. Oceanogr. Methods*, 6(5), 190–199, doi:10.4319/lom.2008.6.190, 2008.
- 880 Moreau, S., Kauko, H. M., Ryan-Keogh, T., Singh, A. and Bratbak, G.: Southern Ocean Ecosystem cruise 2019  
881 biogeochemistry [Data set], Norwegian Polar Institute, doi:10.21334/npolar.2021.28fbddd2, 2020.
- 882 Nöthig, E.-M., Assmy, P., Klaas, C. and Scharek, R.: Phyto- and protozooplankton in polar waters, in *Biological*  
883 *Studies in Polar Oceans: Exploration of Life in Icy Waters*, edited by G. Hempel and I. Hempel, pp. 65–73,  
884 *Wirtschaftsverlag NW, Bremerhaven, Germany.*, 2009.
- 885 Oksanen, J., Blanchet, F. G., Friendly, M., Kindt, R., Legendre, P., McGlenn, D., Minchin, P. R., O’Hara, R. B.,  
886 Simpson, G. L., Solymos, P., Stevens, M. H. H., Szoecs, E. and Wagner, H.: *vegan: Community Ecology*  
887 *Package*, [online] Available from: <https://cran.r-project.org/package=vegan>, 2017.
- 888 Pančić, M. and Kjørboe, T.: Phytoplankton defence mechanisms: traits and trade-offs, *Biol. Rev.*, 93(2), 1269–  
889 1303, doi:10.1111/brv.12395, 2018.
- 890 Peeken, I.: Photosynthetic pigment fingerprints as indicators of phytoplankton biomass and development in  
891 different water masses of the Southern Ocean during austral spring, *Deep. Res. Part II Top. Stud. Oceanogr.*,  
892 44(1–2), 261–282, doi:10.1016/S0967-0645(96)00077-X, 1997.
- 893 Pollard, R. T., Salter, I., Sanders, R. J., Lucas, M. I., Moore, C. M., Mills, R. A., Statham, P. J., Allen, J. T.,  
894 Baker, A. R., Bakker, D. C. E., Charette, M. A., Fielding, S., Fones, G. R., French, M., Hickman, A. E., Holland,  
895 R. J., Hughes, J. A., Jickells, T. D., Lampitt, R. S., Morris, P. J., Nédélec, F. H., Nielsdóttir, M., Planquette, H.,  
896 Popova, E. E., Poulton, A. J., Read, J. F., Seeyave, S., Smith, T., Stinchcombe, M., Taylor, S., Thomalla, S.,  
897 Venables, H. J., Williamson, R. and Zubkov, M. V.: Southern Ocean deep-water carbon export enhanced by  
898 natural iron fertilization, *Nature*, 457(7229), 577–580, doi:10.1038/nature07716, 2009.
- 899 Poulin, M., Daugbjerg, N., Gradinger, R., Ilyash, L., Ratkova, T. and von Quillfeldt, C.: The pan-Arctic  
900 biodiversity of marine pelagic and sea-ice unicellular eukaryotes: A first-attempt assessment, *Mar. Biodivers.*,  
901 41(1), 13–28, doi:10.1007/s12526-010-0058-8, 2011.
- 902 R Core Team: *R: A language and environment for statistical computing*, R Foundation for Statistical Computing,  
903 Vienna, Austria, 2017. R version 3.4.2. <https://www.R-project.org/>
- 904 Rembauville, M., Briggs, N., Ardyna, M., Uitz, J., Catala, P., Penkerch, C., Poteau, A., Claustre, H. and Blain,  
905 S.: Plankton assemblage estimated with BGC-Argo floats in the Southern Ocean: Implications for seasonal  
906 successions and particle export, *J. Geophys. Res. Ocean.*, 122(10), 8278–8292, doi:10.1002/2017JC013067,  
907 2017.
- 908 Roy, S., LLewellyn, C. A., Egeland, E. S. and Johnsen, G., Eds.: *Phytoplankton Pigments - Characterization,*  
909 *Chemotaxonomy and Applications in Oceanography*, 1. edition., Cambridge University Press, Cambridge., 2011.
- 910 Sachs, O., Sauter, E. J., Schlüter, M., Rutgers van der Loeff, M. M., Jerosch, K. and Holby, O.: Benthic organic



- 911 carbon flux and oxygen penetration reflect different plankton provinces in the Southern Ocean, *Deep. Res. Part I*  
912 *Oceanogr. Res. Pap.*, 56(8), 1319–1335, doi:10.1016/j.dsr.2009.02.003, 2009.
- 913 Schulz, I., Montresor, M., Klaas, C., Assmy, P., Wolzenburg, S., Gauns, M., Sarkar, A., Thiele, S., Wolf-  
914 Gladrow, D., Naqvi, W. and Smetacek, V.: Remarkable structural resistance of a nanoflagellate-dominated  
915 plankton community to iron fertilization during the Southern Ocean experiment LOHAFEX, *Mar. Ecol. Prog.*  
916 *Ser.*, 601, 77–95, doi:10.3354/meps12685, 2018.
- 917 Smetacek, V., Assmy, P. and Henjes, J.: The role of grazing in structuring Southern Ocean pelagic ecosystems  
918 and biogeochemical cycles, *Antarct. Sci.*, 16(4), 541–558, doi:10.1017/S0954102004002317, 2004.
- 919 Smetacek, V., Klaas, C., Strass, V. H., Assmy, P., Montresor, M., Cisewski, B., Savoye, N., Webb, A.,  
920 D’Ovidio, F., Arrieta, J. M., Bathmann, U., Bellerby, R., Berg, G. M., Croot, P., Gonzalez, S., Henjes, J.,  
921 Herndl, G. J., Hoffmann, L. J., Leach, H., Losch, M., Mills, M. M., Neill, C., Peeken, I., Röttgers, R., Sachs, O.,  
922 Sauter, E., Schmidt, M. M., Schwarz, J., Terbrüggen, A. and Wolf-Gladrow, D.: Deep carbon export from a  
923 Southern Ocean iron-fertilized diatom bloom, *Nature*, 487(7407), 313–319, doi:10.1038/nature11229, 2012.
- 924 de Steur, L., Holland, D. M., Muench, R. D. and McPhee, M. G.: The warm-water “Halo” around Maud Rise:  
925 Properties, dynamics and impact, *Deep Sea Res. I*, 54, 871–896, doi:10.1016/j.dsr.2007.03.009, 2007.
- 926 Saavedra-Pellitero, M., Baumann, K.-H., Flores, J.-A. and Gersonde, R.: Biogeographic distribution of living  
927 coccolithophores in the Pacific sector of the Southern Ocean, *Mar. Micropaleontol.*, 109, 1–20, 2014.
- 928 Tran, S., Bonsang, B., Gros, V., Peeken, I., Sarda-Esteve, R., Bernhardt, A. and Belviso, S.: A survey of carbon  
929 monoxide and non-methane hydrocarbons in the Arctic Ocean during summer 2010, *Biogeosciences*, 10(3),  
930 1909–1935, doi:10.5194/bg-10-1909-2013, 2013.
- 931 Tréguer, P., Bowler, C., Moriceau, B., Dutkiewicz, S., Gehlen, M., Aumont, O., Bittner, L., Dugdale, R., Finkel,  
932 Z., Iudicone, D., Jahn, O., Guidi, L., Lasbleiz, M., Leblanc, K., Levy, M. and Pondaven, P.: Influence of diatom  
933 diversity on the ocean biological carbon pump, *Nat. Geosci.*, 11(1), 27–37, doi:10.1038/s41561-017-0028-x,  
934 2018.
- 935 Trull, T. W., Passmore, A., Davies, D. M., Smit, T., Berry, K. and Tilbrook, B.: Distribution of planktonic  
936 biogenic carbonate organisms in the Southern Ocean south of Australia: A baseline for ocean acidification  
937 impact assessment, *Biogeosciences*, 15(1), 31–49, doi:10.5194/bg-15-31-2018, 2018.
- 938 Vallina, S. M., Follows, M. J., Dutkiewicz, S., Montoya, J. M., Cermeno, P. and Loreau, M.: Global relationship  
939 between phytoplankton diversity and productivity in the ocean, *Nat. Commun.*, 5, 4299,  
940 doi:10.1038/ncomms5299, 2014.
- 941 Venables, W. N. and Ripley, B. D.: *Modern applied statistics with S*, 4. edition., Springer, New York., 2002.
- 942 Vernet, M., Geibert, W., Hoppema, M., Brown, P. J., Haas, C., Hellmer, H. H., Jokat, W., Jullion, L., Mazloff,  
943 M., Bakker, D. C. E., Brearley, J. A., Croot, P., Hattermann, T., Hauck, J., Hillenbrand, C.-D., Hoppe, C. J. M.,  
944 Huhn, O., Koch, B. P., Lechtenfeld, O. J., Meredith, M. P., Naveira Garabato, A. C., Nöthig, E.-M., Peeken, I.,  
945 van der Loeff, M. M. R., Schmidtko, S., Schröder, M., Strass, V. H., Torres-Valdés, S. and Verdy, A.: The



- 946 Weddell Gyre, Southern Ocean: Present knowledge and future challenges, *Rev. Geophys.*, 57(3), 623–708,  
947 doi:10.1029/2018RG000604, 2019.
- 948 Wright, S.: Chemtax version 1.95 for calculating the taxonomic composition of phytoplankton populations,  
949 Australian Antarctic Data Centre, Accessed: 2020-11-27, doi:10.4225/15/59fff1c5ea8fc, 2008.
- 950 Wright, S. W., van den Enden, R. L., Pearce, I., Davidson, A. T., Scott, F. J. and Westwood, K. J.:  
951 Phytoplankton community structure and stocks in the Southern Ocean (30-80°E) determined by CHEMTAX  
952 analysis of HPLC pigment signatures, *Deep. Res. Part II Top. Stud. Oceanogr.*, 57(9–10), 758–778,  
953 doi:10.1016/j.dsr2.2009.06.015, 2010.
- 954 Zapata, M., Jeffrey, S. W., Wright, S. W., Rodríguez, F., Garrido, J. L. and Clementson, L.: Photosynthetic  
955 pigments in 37 species (65 strains) of Haptophyta: Implications for oceanography and chemotaxonomy, *Mar.*  
956 *Ecol. Prog. Ser.*, 270, 83–102, doi:10.3354/meps270083, 2004.
- 957